applied optics

Characterization of suspended particulate matter in contrasting coastal marine environments with angle-resolved polarized light scattering measurements

Daniel Koestner,[1,*] Dariusz Stramski,[2] and Rick A. Reynolds[2]

[1]Naval Research Laboratory, Washington, DC 20375, USA
[2]Marine Physical Laboratory, Scripps Institution of Oceanography, University of California San Diego, La Jolla, California 92093-0238, USA
*Corresponding author: daniel.koestner.ctr@nrl.navy.mil

Received 24 August 2021; revised 18 November 2021; accepted 19 November 2021; posted 19 November 2021; published 13 December 2021

Optical proxies based on light scattering measurements have potential to improve the study and monitoring of aquatic environments. In this study, we evaluated several optical proxies for characterization of particle mass concentration, composition, and size distribution of suspended particulate matter from two contrasting coastal marine environments. We expanded upon our previous study of Southern California coastal waters, which generally contained high proportions of organic particles, by conducting angle-resolved polarized light scattering measurements in predominantly turbid and inorganic-particle dominated Arctic coastal waters near Prudhoe Bay, Alaska. We observed that the particulate backscattering coefficient b_{bp} was the most effective proxy for the mass concentration of suspended particulate matter (SPM) when compared with particulate scattering and attenuation coefficients b_p and c_p. Improvements were seen with b_{bp} as a proxy for the concentration of particulate organic carbon (POC), although only if particulate assemblages were previously classified in terms of particle composition. We found that the ratio of polarized-light scattering measurements at 110° and 18° was superior in performance as a proxy for the composition parameter POC/SPM in comparison to the particulate backscattering ratio b_{bp}/b_p. The maximum value of the degree of linear polarization $\mathrm{DoLP}_{p,\max}$ observed within the range of scattering angles 89°–106° was found to provide a reasonably good proxy for a particle size parameter (i.e., 90th percentile of particle volume distribution) which characterizes the proportions of small- and large-sized particles. These findings can inform the development of polarized light scattering sensors to enhance the capabilities of autonomous platforms.

https://doi.org/10.1364/AO.441226

1. INTRODUCTION

In situ optical measurements, especially from autonomous platforms, have generally transformed the study of aquatic ecosystems by providing unique opportunities to monitor biogeochemical processes in fresh- and salt-water environments at unsurpassed temporal and spatial scales of observation [1–5]. Coastal environments are of particular interest due to high levels of interaction between humans and these environments, which generally provide ecological services of significant importance such as carbon sequestration, supporting fisheries, storm protection, and providing aesthetic services of most relevance to tourism industries [6]. Accurate measurements of suspended particulate material, living or nonliving, in these coastal waters are therefore of great importance when considering the health of such coastal ecosystems (e.g., [7,8]). Understanding more about the nature of particulate material can also further improve our assessments of these waters in a broader context. The advancement of a broad range of scientific topics in coastal environments, from biogeochemical models to satellite remote sensing, requires more complete measurements of the inherent optical properties (IOPs) of natural assemblages of aquatic particles. These IOPs describe the interactions of light with particles suspended in aquatic medium, which are dependent solely on the physical and chemical properties of the particles themselves as well as the medium, especially its refractive index [9,10]. Coastal waters, however, present challenges for optically-based assessments because of the optically complex nature of particle assemblages with various origins resulting from terrestrial input and dynamic mixing conditions with offshore waters [11–13]. Furthermore, rapidly changing coastal environments, such as those found in remote northern polar latitudes, present additional challenges because of limited availability of optical

measurements and could benefit from routine monitoring to help understand ecological impacts associated with climate change [14,15].

Light scattering measurements provide a unique approach for monitoring coastal environments because they can provide useful information about complex particle assemblages through various signatures associated with scattering properties, e.g., magnitude, spectral behavior, angular patterns, and polarization properties [16]. Additionally, from a practical point of view, scattering measurements can be implemented into routine use through development of appropriate sensors. For example, *in situ* scattering sensors providing a measurement at one or a few scattering angles at a single or several light wavelengths (e.g., YSI turbidity sensors, Sea-Bird Scientific's Environmental Characterization Optics sensors, or HOBI Labs' HydroScat sensors) have been used to estimate the mass concentrations of suspended particulate matter (e.g., [17–20]) and particulate organic carbon (e.g., [21–25]) as well as properties associated with particle size distribution (e.g., [26–29]). More advanced light scattering approaches based on angular distribution of light scattering, including spectral and polarization properties, have the potential to be used for differentiating characteristic features of aquatic particulate assemblages associated with their organic versus inorganic composition and size distribution [9,16]. Theoretically-based inversions of measured light scattering at near-forward scattering angles can provide useful information about particle size distribution [30], while including nearly the full distribution of scattering angles in such inversions can improve assessment in terms of particle size distribution and composition [31]. The ratio of the magnitude of particulate scattering integrated over backward angles to total particulate scattering magnitude has also been theorized to be sensitive to size distribution and composition of marine particles [32,33]. This particulate backscattering ratio has been observed to be a potentially useful proxy for particulate compositional characteristics of seawater [34–37], although more work is needed to validate its use as a robust proxy for specific compositional parameters [38]. It is also expected that spectral characteristics of light scattering by natural assemblages of particles can be useful for identifying particulate properties [29,38–42]. These previous studies are either based on the use of scattering parameters inferred as a difference between the beam attenuation and absorption measurements or are limited in terms of measured scattering angles or in characterization of particulate properties such as size distribution and composition. Finally, measurements of the polarization properties of light scattered by particles may aid in the identification and differentiation between different types of particles, such as phytoplankton species or minerals, which are present in complex natural assemblages [43–48]. However, relatively few measurements exist of a wide angular distribution of polarized light scattered by natural assemblages of aquatic particles with concurrent comprehensive characterization of the particulate assemblage in terms of particle composition and size distribution [35,49,50].

Whereas we recently demonstrated the potential usefulness of light scattering proxies based on angle-resolved polarized light scattering measurements for estimating characteristic features associated with particle composition and size distribution, these proxies were analyzed with water samples from one coastal region of San Diego, California [49]. It is of interest to investigate if such proxies can have more general applicability in a variety of aquatic environments. In the present study we examine relationships between light scattering and particle characteristics for coastal Arctic waters of the central Beaufort Sea in the region of Prudhoe Bay, Alaska, where considerable terrestrial input from various river systems generally results in inorganic-dominated particulate assemblages. We combine these observations from Prudhoe Bay with previously collected data from San Diego coastal waters in which water samples were typically dominated by organic particles. This enabled the evaluation of relationships between light scattering and particle characteristics over a wide range of particle compositions from two different coastal marine environments.

The current study utilizes the LISST-VSF instrument to measure angle-resolved polarized light scattering by particles suspended in seawater at a single wavelength of 532 nm. This commercially available instrument is increasingly being used to study marine particles [51–56], including our recent studies [35,49,57]. *In situ* light scattering measurements are prone to undesired multiple scattering effects if turbidity of water exceeds a certain level [16,54,58–60]. In this study, we first examine a correction for multiple scattering based on laboratory measurements with mineral particles of natural origin. Second, we present measurement results related to field work in nearshore waters around Prudhoe Bay, including the angular distributions of linearly polarized light scattered by assemblages of aquatic particles. Finally, we describe relationships between light scattering parameters and particulate characteristics for contrasting particle assemblages from two different coastal environments, and we assess different optical proxies for predicting characteristics associated with the concentration, composition, and size distribution of suspended particulate material.

2. METHODS

In addition to previously reported results from San Diego coastal waters, this study includes new *in situ* measurements obtained from coastal Arctic waters of the Beaufort Sea near Prudhoe Bay, Alaska. We describe methods relevant to the coastal Arctic field work below, whereas all methodology associated with benchtop measurements of San Diego coastal samples can be found in a previous publication [49].

A. Field Sampling

The Arctic field data were collected early September 2018 and August 2019 in the nearshore waters of the central Beaufort Sea in the vicinity of Prudhoe Bay, Alaska, onboard R/V Ukpik. Figure 1 shows a map of the general region. A total of 12 station locations were surveyed, spanning near the Kuparuk and Sagavanirktok River mouths (KO and SO, respectively) to 80 km offshore (UPE80), but most stations were within 10 km of shoreline (Fig. 1). Some locations were visited on multiple occasions, either a few days apart or one year apart, and are denoted with an additional letter b or c to indicate repeated visits to approximately the same location.

Depth profiles were performed at each station visit with an optical package containing several instruments. Of most

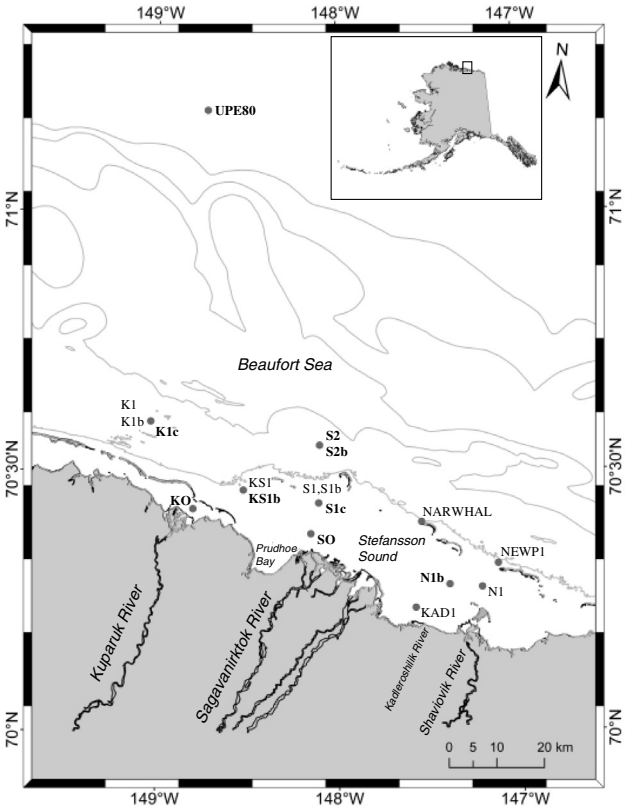

Fig. 1. Map of Prudhoe Bay, Alaska region with station locations indicated with black circles. Station names are displayed, and station locations in 2018 are denoted using regular font while stations in 2019 are denoted using boldface. Isobath interval is 10 m.

interest to the current study, the optical package contained a LISST-VSF (Sequoia Scientific), SBE 49 FastCAT conductivity, temperature, and depth (CTD) sensor (Sea-Bird Scientific), and ac-s (Sea-Bird Scientific). During each cast the optical package remained at a near-surface and near-bottom depth for approximately 5–10 min to accommodate the various sample rates of instruments and to acquire a statistically representative set of measurements. Following *in situ* optical measurements, 5L Niskin bottles were deployed at surface and near-bottom depths corresponding with extended acquisition of optical data. A discrete water sample at a given depth was collected using as many as three Niskin bottles, and the collected water was combined in a larger carboy before subsampling for particulate analysis. Surface sampling depths were typically 1 m below the sea surface. Near-bottom sampling depths typically ranged from 5 to 15 m and were generally a few meters above the seafloor as estimated from the vessel's sonar system. Only surface water was collected at KO and SO stations and near-bottom water at UPE80 was collected 50 m below surface. Surface water from S1 was not included in the current study due to poor quality of the LISST-VSF measurements. In summary, 18 stations were sampled, 15 of which included surface and near-bottom measurements, for a total of 33 samples for particle and optical characterization. For simplicity, we refer to near-bottom depth as "bottom" and all Arctic field data as "Prudhoe Bay."

B. Particle Characterization

Depending on particle concentration, approximately 100–1400 mL of seawater were filtered through 25 mm diameter Whatman glass fiber filters (GF/F) at low vacuum (<120 mm Hg) using pre-combusted, pre-rinsed, and pre-weighted filters for the determination of the dry mass concentration of suspended particulate matter (SPM) and pre-combusted filters for the determination of concentration of particulate organic carbon (POC) following standard methodology [61,62]. Filtrations were generally completed within a few hours after sampling when the boat was either anchored or docked, and water remained on deck at ambient air temperature (0°C–10°C) protected from sunlight in the interim. Following collection of particulate material, SPM and POC filters were dried in a small oven at about 55°C and stored for post-cruise laboratory-based analysis. Blank filters for SPM were randomly prepared by filtering 25–50 mL of 0.2 μm filtered deionized water through pre-combusted, pre-rinsed, and pre-weighed 25 mm diameter GF/F filters to correct for potential error in SPM associated with contamination during various stages of sample collection and analysis. Additional blank filters for POC were also prepared utilizing GF/F filtered seawater collected from a few stations to enable adjustment of POC for adsorption of dissolved organic carbon on filters [22,63]. These corrections resulted in an average reduction of 5% for SPM and 11% for POC. Duplicate filters were collected for both SPM and POC. In most cases, replicates were averaged to determine a final estimate of SPM and POC at each station's surface and bottom depths. Coefficients of variation between replicates of SPM and POC were on average 3% and 7%, respectively.

Approximately 50–1000 mL of seawater were filtered through 25 mm GF/F filters for measurements of spectral absorption coefficient of particles $a_p(\lambda)$ [m^{-1}]. After collection of particulate material, filters were immediately stored in liquid nitrogen until further post-cruise processing in the lab. Measurements were made in the spectral range 300–850 nm with 1 nm interval using a Lambda 18 UV/VIS spectrophotometer (Perkin Elmer) equipped with a 15 cm integrating sphere (RSA-PE-18, Labsphere) and with the filter placed inside the sphere (e.g., [64–66]). Following the measurement of $a_p(\lambda)$, the sample filters were treated with methanol and remeasured to determine the spectral absorption coefficient of non-algal (more specifically, depigmented) particles [67], denoted as $a_d(\lambda)$. The calculation of $a_p(\lambda)$ and $a_d(\lambda)$ involved use of the path length amplification correction recommended in Stramski *et al*. [66] for the inside-sphere configuration of the filter-pad method. A final adjustment was made to $a_d(\lambda)$ to ensure that $a_d(\lambda)$ and $a_p(\lambda)$ values matched in the near-infrared spectral region (775–800 nm). The spectral absorption coefficient of phytoplankton was then calculated as $a_{ph}(\lambda) = a_p(\lambda) - a_d(\lambda)$.

Measurements of forward scattering from the LISST-VSF ring detectors were used to estimate the particle size distribution (PSD). The approach utilized Fraunhofer diffraction theory to invert forward scattering signal to produce a PSD in terms of particle volume concentration for 32 logarithmically spaced bins of equivalent spherical diameters D from 1–160 μm (processing code provided by Sequoia Scientific). This is a similar approach often used with other LISST instruments

and provides reasonable estimates of the PSD for natural particle assemblages of aquatic origin [30,68–70]. We provide a graphical representation of the density function of particle number distribution $N(D)$ [$\mathrm{cm}^{-3}\ \mu\mathrm{m}^{-1}$], which results from the normalization of particle number concentration in each size bin by the width of each bin. We also depict PSDs using cumulative distribution functions for particle volume CDF_V, which are determined by dividing the cumulative particle volume concentration by the total particle volume.

For the current study, we consider two parameters to quantify composition of particulate matter; POC/SPM as an indicator of the contributions of organic versus inorganic particles, and the fraction $a_{ph}(\lambda)/a_p(\lambda)$ at $\lambda = 440$ nm as an indicator of the prevalence of phytoplankton in the sample. The high values of POC/SPM indicate the prevalence of organic particles, and the low values indicate the prevalence of inorganic particles. Whereas high values of POC/SPM do not distinguish between phytoplankton and detrital organic material, high values of $a_{ph}(440)/a_p(440)$ suggest the prevalence of phytoplankton and low values suggest prevalence of non-phytoplankton particles. These metrics have been used previously to assess composition of natural assemblages of marine particles (e.g., [20,36,38,42,49,57]). In terms of parameterizing the particle size distribution, we choose the 90th percentile of the volume distribution D_V^{90} [μm] as an indicator of the relative proportions of small- versus large-sized particles. We utilize particle volume distributions because relatively rare large-sized particles can be underrepresented in particle area or number size distributions and because the particle volume is more directly related to intraparticle concentration of biogeochemically important constituents such as carbon or pigments. In particular, the size parameter D_V^{90} has been shown to be potentially useful in the analysis of relationships between optical and particle size properties in seawater [42,57]. In this study, D_V^{90} was calculated for each station depth from the CDF_V for 20 size bins with lower bin edge of 2.0 μm and upper bin edge of 54.4 μm to be most compatible with the 2–60 μm size range used in our previous study of San Diego coastal waters [49]. In determining D_V^{90}, the CDF_V was linearly interpolated in $\log_{10}$-space because of the coarsely spaced binning of the PSD provided from the LISST-VSF measurements.

C. Light Scattering Measurements

In situ measurements of angle-resolved polarized light scattering in Arctic waters were made with the LISST-VSF instrument. The LISST-VSF model used in this study measures scattering within the range of scattering angle ψ from 0.08° to 150° at light wavelength λ of 532 nm (in vacuum) with an incident laser beam 3.2 mm in diameter. Each measurement takes approximately 4 s and consists of two scans of a 15 cm path within the sample, each with different linear polarization state of the incident beam, i.e., perpendicular ⊥ and parallel ∥ to a reference plane. Forward scattering in the range 0.08°–14° is measured with 32 logarithmically spaced ring detectors with no polarizing elements while the angular range 15°–150° is measured at 1° resolution with a roving eyeball sensor that further partitions scattered light into perpendicular and parallel polarized components for detection by two photomultiplier tubes (PMTs). Transmitted light is also detected using a forward detector with 0.04° acceptance angle for the determination of the beam attenuation coefficient c. The instrument configuration enables estimates of the volume scattering function β and the degree of linear polarization of scattered light DoLP in addition to the directly measured four incident and detector polarization combinations: $\beta^{\perp\parallel}$, $\beta^{\perp\perp}$, $\beta^{\parallel\perp}$, and $\beta^{\parallel\parallel}$. In the latter four symbols, the first and second superscript characters denote incident and detected polarization state, respectively. Note that all light scattering measurements are functions of scattering angle ψ defined with 0° as the initial direction of light propagation, but it is not included in most representations for brevity. More detailed description of the instrument can be found in previous publications [35,49], and Table 1 includes descriptions of the LISST-VSF measurements in terms of scattering, or Mueller, matrix elements. We briefly mention here that the degree of linear polarization of light scattered by particles DoLP_p describes the proportion of linearly polarized light relative to total intensity of the scattered light beam. For various assemblages of particles including suspended marine particles and when the incident light beam is unpolarized, this quantity can be derived from scattering matrix elements p_{11} and p_{12} (Table 1), which require measurements involving linear polarization [47,71].

To determine angle-resolved polarized light scattering associated with only particles, and denoted with a subscript "p" we used a combination of benchtop measurements and theoretical estimates of molecular scattering by pure seawater. Benchtop measurements of 0.2 μm filtered deionized and degassed water were used as a baseline for only ring and transmission detectors, and they were subtracted from *in situ* measured results. This baseline is used to primarily remove scattering and attenuation associated with receiver window optics under the assumption that additional scattering and absorption associated with temperature and salinity of pure seawater is negligible for near-forward scattering and beam attenuation. An average of two baselines measured before the 2018 deployments and after the 2019 deployments was used. For roving eyeball sensor angles, theoretical estimates of scattering by pure seawater were subtracted from measurement results because contribution of pure seawater to scattering can be significant for backwards angles, especially in clear waters [52,72,73]. The theoretical estimates of scattering were determined using salinity and temperature measured by the CTD at corresponding station depths and equations found in Zhang *et al*. [73]. Additional salinity dependence of the depolarization ratio was included when calculating theoretical light scattering properties of pure seawater; $\partial = 0.039 + 0.0001S$, where ∂ is depolarization ratio and S is salinity in practical salinity units (PSU) [74].

Manufacturer updates in 2017 to LISST-VSF firmware, processing code, and ring detector optics resulted in a few changes relevant to current measurements as compared to our earlier study of San Diego coastal waters. Ring angles have been shifted slightly (to 0.08°–14° from 0.09°–15°), and a new autogain feature was introduced that automatically cycles through 10 PMT gain settings to determine optimal gain setting for current measurement series. Several studies have identified necessary calibration corrections to manufacturer provided processing to improve the accuracy of results [35,49,54,72]. Although the approaches vary somewhat, they

Table 1. Relevant Symbols and their Descriptions

Symbol	Description
Light scattering variables	
ψ	Scattering angle with 0 defined as direction of initial propagation [deg]
S_f and α	Instrument-specific calibration constants
p_{11}, p_{12}, and p_{22}	Elements of the 4×4 scattering, or Mueller, matrix describing polarized light scattering by particles
$\beta_p^{\perp\parallel}$	LISST-VSF measurement with incident light polarized perpendicular and detected light polarized parallel [m^{-1} sr^{-1}]; $S_f[p_{11}(\psi) - p_{12}(\psi) + \cos 2\psi(p_{12}(\psi) - p_{22}(\psi))]$
$\beta_p^{\perp\perp}$	LISST-VSF measurement with incident light polarized perpendicular and detected light polarized perpendicular [m^{-1} sr^{-1}]; $\frac{S_f}{\alpha}[p_{11}(\psi) - p_{12}(\psi) - \cos 2\psi(p_{12}(\psi) - p_{22}(\psi))]$
$\beta_p^{\parallel\parallel}$	LISST-VSF measurement with incident light polarized parallel and detected light polarized parallel [m^{-1} sr^{-1}]; $S_f[p_{11}(\psi) + p_{12}(\psi) + \cos 2\psi(p_{12}(\psi) + p_{22}(\psi))]$
$\beta_p^{\parallel\perp}$	LISST-VSF measurement with incident light polarized parallel and detected light polarized perpendicular [m^{-1} sr^{-1}]; $\frac{S_f}{\alpha}[p_{11}(\psi) + p_{12}(\psi) - \cos 2\psi(p_{12}(\psi) + p_{22}(\psi))]$
β_p	Particulate volume scattering function [m^{-1} sr^{-1}]; $b_p \times p_{11} = \frac{1}{4}[\beta_p^{\perp\parallel}(\psi) + \beta_p^{\parallel\parallel}(\psi) + \beta_p^{\perp\perp}(\psi) + \beta_p^{\parallel\perp}(\psi)]$
DoLP_p	Degree of linear polarization of light scattered by particles; $-\frac{p_{12}}{p_{11}} = -\frac{\frac{1}{4}\left[\beta_p^{\parallel\perp}(\psi) + \beta_p^{\parallel\parallel}(\psi) - \left(\beta_p^{\perp\parallel}(\psi) + \beta_p^{\perp\perp}(\psi)\right)\right]}{\beta_p(\psi)}$
$\mathrm{DoLP}_{p,\max}$	Maximum value of $\mathrm{DoLP}_p(\psi)$
b_p	Particulate scattering coefficient [m^{-1}]; $2\pi \int_{0°}^{180°} \beta_p(\psi)\sin(\psi)\mathrm{d}\psi$
b_{bp}	Particulate backscattering coefficient [m^{-1}]; $2\pi \int_{90°}^{180°} \beta_p(\psi)\sin(\psi)\mathrm{d}\psi$
Model-assessment variables	
N	Number of samples
x_i or y_i	Measured value for sample i of N
$\bar{x}$ or $\bar{y}$	Mean value; $\bar{x} = \frac{1}{N}\sum_{i=1}^{N} x_i$, and likewise for $\bar{y}$
O_i or P_i	Observed or model-predicted value for sample i of N
R	Pearson correlation coefficient; $\frac{\sum_{i=1}^{N}(x_i - \bar{x})(y_i - \bar{y})}{\sqrt{\sum_{i=1}^{N}(x_i - \bar{x})^2}\sqrt{\sum_{i=1}^{N}(y_i - \bar{y})^2}}$
Md	Median operator
RMSD	Root-mean-square deviation; $\sqrt{\frac{1}{N}\sum_{i=1}^{N}(P_i - O_i)^2}$
MdAPD	Median absolute percent difference; $Md\left\|\frac{P_i - O_i}{O_i}\right| \times 100\%$
MdSA	Median symmetric accuracy; $(10^{Md\left\|\log_{10}\frac{P_i}{O_i}\right|} - 1) \times 100\%$
MdLQ	Median log-accuracy ratio; $Md\left\|\log_{10}\frac{P_i}{O_i}\right|$

all utilize empirical corrections based on Mie scattering simulations and measurements with nearly monodisperse assemblages of standard polystyrene bead suspensions. For the current study, the calibration corrections were developed based on measurements made with 200, 270, 400, and 700 nm polystyrene bead suspensions, with the bulk of the corrections developed using 200 nm polystyrene beads given the advantages of the use of a featureless angular scattering pattern of such beads. More details regarding development of these corrections can be found in our previous publications [35,49]. Although the Koestner *et al*. [49] correction approach results in one set of corrections for all β_p, DoLP_p, and four eyeball measurement combinations, we chose the method for corrected β_p and DoLP_p from Koestner *et al*. [35], which determines corrections for β_p and DoLP_p after combining all eyeball measurements. The two approaches for corrected β_p and DoLP_p agree well for polystyrene bead suspensions but sometimes differ for natural seawater samples. When comparing the two correction approaches for various seawater samples, similarities in corrected β_p were observed (<5% difference between approaches); however, differences in corrected DoLP_p were often more substantial. The Koestner *et al*. [49] approach increased maximum values of DoLP_p (i.e., $\mathrm{DoLP}_{p,\max}$) by ~0.05−0.15 when compared with results obtained with Koestner *et al*. [35] corrections. In the current study, it is assumed that the simpler approach for DoLP_p corrections is preferable, as DoLP_p is already in good agreement with theory for polystyrene beads without any correction to eyeball measurements [35]. Owing to recent manufacturer updates, the correction factors for β_p were less significant than what was found in Koestner *et al*. [35], ranging approximately from 0.85 to 1.12 depending on scattering angle. Additive corrections to DoLP_p were about the same as what was found in Koestner *et al*. [35], e.g., about 0.05 increase in DoLP_p near 90°.

The polystyrene bead measurements used in developing corrections were also used to identify relative PMT factor α and PMT scaling factors S_f for use with *in situ* acquired data. The value of α was fixed at 0.97 for all field data processing. Scaling factors for our field data were based on polystyrene bead measurements at four PMT gain settings and linearly extrapolated in $\log_{10}$-space to additional PMT gain settings as recommended

by Hu *et al*. [72]. The *in situ* measurements in Arctic waters were made in very low temperatures near 0°C, so we include an additional adjustment of the benchtop-derived scale factors based on the field measurements to account for changes in instrument performance associated with temperature. This adjustment factor was 0.85 and fixed for all PMT gain settings.

During extended sampling at surface and bottom depths of each station location, 40–200 measurements were collected, and about 10% were removed following quality control of data. Median values were determined from remaining data at each scattering angle, adjusted using the calibration correction functions for β_p, DoLP_p, and four eyeball measurement combinations, and finally smoothed, first with a 3°, then twice with a 5° moving average. We note here that we observed reasonable convergence to median values of β_p and DoLP_p after 30–60 measurements depending on scattering angle and station.

D. Development of Multiple Scattering Corrections

In this section, we describe the development of an important methodological aspect of the current study associated with multiple scattering and the LISST-VSF instrument. First, we provide some useful background information about multiple scattering, next we describe laboratory experiments used in the development of empirically-based corrections for multiple scattering, and then we describe the formulation of the final operational multiple scattering corrections used in the current study.

Undesired effects of multiple scattering can be problematic for light scattering meters in turbid coastal environments (e.g., [54,59]). In these cases, once scattered light can be additionally scattered and reenter the viewing detector to artificially change the magnitude of scattering for any given scattering angle. Multiple scattering effects for light scattering meters are complex and depend on many factors including particle concentration, particle scattering characteristics, and instrument geometry. Given the relatively long path length of the LISST-VSF instrument and its scanning detector system (13–17.5 cm), these effects are likely to be encountered during *in situ* measurements in coastal environments such as the investigated Arctic waters. Furthermore, the LISST-VSF data processing utilizes an attenuation correction to account for losses along the path to and from the scattering volume where the incident beam intersects the detector's viewing angle. The impact of multiple scattering on this correction for attenuation losses is unclear.

A general rule for single scattering is $\tau(1-g) \ll 1$, where τ is the optical thickness determined as $c \times r$, c is beam attenuation coefficient in m^{-1}, r is path length in m, and g is average cosine of scattering phase function [16]. For the longest path of the LISST-VSF ($r = 17.5$ cm), the single scattering regime is expected for $c \ll 57\ \mathrm{m}^{-1}$, assuming a strongly forward peaking phase function representative of typical seawater ($g = 0.9$). Recently, Sandven *et al*. [54] found that multiple scattering effects may become noticeable for scattering coefficient $b > 2\ \mathrm{m}^{-1}$ based on comparisons of measurements with a LISST-VSF and a LISST-200X. We thus consider multiple scattering effects for the LISST-VSF may become apparent around $c = 2{-}6\ \mathrm{m}^{-1}$ and acknowledge that there will not be a perfect cutoff for all seawater samples given the complex and variable nature of marine particle assemblages.

Benchtop experiments were performed to develop empirical corrections for multiple scattering effects observed with the LISST-VSF instrument so that field measurements could be adjusted to appropriately remove effects of multiple scattering as such:

$$B_p = \frac{\beta_p^+}{E^\beta}, \tag{1}$$

$$\mathrm{DoLP}_p = \mathrm{DoLP}_p^+ + E^{\mathrm{DoLP}}, \tag{2}$$

where E^β and E^{DoLP} are angle-dependent multiple scattering correction functions and superscript "+" denotes original results before multiple scattering adjustment. These experiments involved measurements of marine particles of natural origin that had been diluted to obtain various particle concentrations in LISST-VSF benchtop chamber with beam attenuation coefficients ranging from $1.8\ \mathrm{m}^{-1}$ to $14\ \mathrm{m}^{-1}$. Dilution-corrected results were compared to determine the change in measured signal as a result of increasing sample turbidity and multiple scattering. We evaluated β_p, DoLP_p, all four polarization measurement combinations, and uncalibrated ring counts used for the determination of PSD. Note that we examined final processed data based on 100–200 measurements, which have undergone the quality control and smoothing outlined in previous section.

One series of dilutions utilized natural particles of glacial origin, which had been collected from the meltwater of glacial material originally retrieved from the shores along Maxwell Bay near King George Island, Antarctica. An additional sample from Los Peñasquitos Lagoon, San Diego County, California, was also evaluated. Dilutions of the glacial meltwater sample were made with 0.2 μm filtered deionized and degassed water, while dilutions of the Los Peñasquitos Lagoon sample were made with GF/F filtrate to minimize effects associated with relatively high light absorption of dissolved material in the sample. In both cases, baseline measurements of the dilution water were subtracted from sample measurements to investigate only scattering and attenuation by particles. An example of dilution-corrected β_p for natural particles of glacial origin is shown in Fig. 2(a). The lowest particle concentration was assumed to produce negligible multiple scattering, and the dilution-corrected values from these measurements were treated as the expected values (i.e., unaffected by multiple scattering) for comparison with other dilution-corrected β_p values determined from measurements with higher particle concentrations. Multiple scattering effects were within reasonable dilution error of about 5% and considered negligible for the beam transmission detector, and hence for the particulate beam attenuation coefficient. This result is consistent with an earlier theoretical study [75].

For each measured c_p value with the LISST-VSF, the angle-dependent multiple scattering correction functions E were computed as the ratio of Expected and Measured values for the cases of β_p, all four polarization measurement combinations, and uncalibrated ring counts, or as the difference of Measured and Expected values for the case of DoLP_p. We assume the

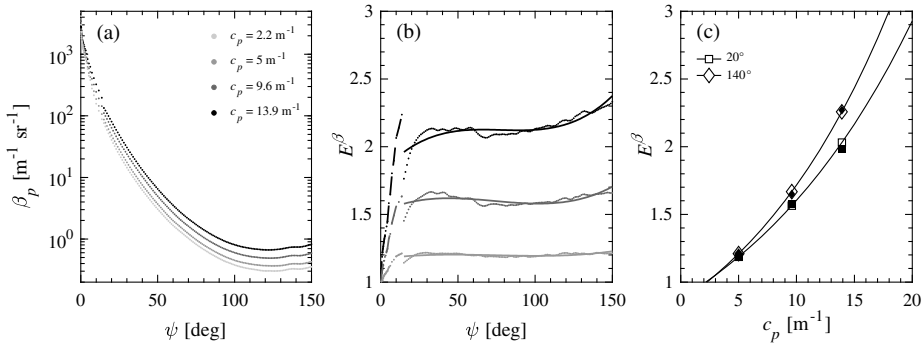

Fig. 2. Development of multiple scattering correction functions using a master particle suspension of mineral particles from glacial meltwater. (a) Dilution-corrected particulate volume scattering functions β_p and (b) E^β (determined as Measured β_p/Expected β_p) as a function of scattering angle ψ based on data in (a) where expected values are from measurements with $c_p = 2.2$ m^{-1}. In (b), small dots are from measurements, while solid lines are third-order polynomial fits to data for $\psi = 15 - 150°$ and dashed lines are cubic-spline fits to data for $\psi < 15°$. Data in (a) and (b) are gray-scaled as indicated in legend in (a) according to c_p of measured diluted master suspension. (c) E^β as exponential functions of c_p at two scattering angles. Filled smaller symbols represent the measured E^β data from (b), while larger empty symbols represent exponential fits of solid lines in (b) at 20° and 140° as indicated in legend.

Expected value, which is unaffected by multiple scattering, corresponds to particle concentration associated with c_p of about 2 m^{-1}. For example,

$$E^\beta(c_p = 5\ \mathrm{m}^{-1},\ \psi = 90°) = \frac{\text{Measured}}{\text{Expected}} = \frac{\beta_p(5\ \mathrm{m}^{-1},\ 90°) \times \mathrm{DF}_2}{\beta_p(2\ \mathrm{m}^{-1},\ 90°) \times \mathrm{DF}_1}, \quad (3)$$

where superscript "β" indicates E is for β_p, and DF_1 and DF_2 are the respective dilution factors based on the total volume in the LISST-VSF chamber divided by the volume of original sample suspension added. Note that ring and eyeball sensor data were treated independently in the fitting routine. The measured E for $\psi = 15°-150°$ were fit with third-order polynomial functions to avoid propagation of uncertainty into the final E from the measured data [e.g., Fig. 2(b)]. The ring E was fit with a cubic spline function forced to 1 at $\psi = 0.08°$, and we excluded $\psi < 1°$ in the fitting because of low signal in the Expected measurement data. The forcing of E to a value of 1 at $\psi = 0.08°$ is reasonable given that negligible multiple scattering effects were observed with the transmission detector. We confirmed that this fitting routine regarding E^β for $\psi < 1°$ only minimally impacted results presented in subsequent sections.

For each angle, an exponential function was fit to the data of the measured E versus measured c_p to aid in the identification of the E most relevant for the measured c_p values from the field [e.g., Fig. 2(c)]. This fit was done while including an anchor value of $E = 1$ (i.e., no multiple scattering correction) at all angles for $c_p = 2$ m^{-1}. Thus, the final E is of the form

$$E(c_p, \psi) = \mathrm{B}(\psi)\, \mathrm{e}^{\mathrm{A}(\psi) \times c_p}, \quad (4)$$

where $A(\psi)$ and $B(\psi)$ are the best-fit coefficients at each angle determined with a total of seven data points.

In the development of the final operational E [Eq. (4)], c_p was used as an independent variable, and it was assumed that c_p was unaffected by multiple scattering and that particulate assemblages had very small or negligible absorption. The latter assumption is reasonable given the origin of the particle assemblages (i.e., glacial meltwater and lagoon water with contributions of dissolved material removed). However, we acknowledge that absorbing particles can impact c_p measurements in the field. Therefore, we adjusted *in situ* c_p measurements by subtracting the contribution of non-water absorption at 532 nm measured by the ac-s spectral absorption sensor attached to our instrument package. For a few cases where ac-s measurements were not available, a non-water absorption value was assumed based on the nearest station in distance and time of c_p measurement. There may be some error propagation into multiple scattering corrections based on uncertainty in non-water absorption derived from ac-s measurements; however, we believe this adjustment is important for coastal samples which may contain strongly absorbing dissolved material. This adjustment lowered c_p by 5%–30% with average adjustment of 17%. The adjusted c_p^* (where $*$ denotes adjustment for absorption) was used to compute the E for application to the final processed data from each station depth. For example,

$$\beta_p(90°) = \frac{\beta_p^+(90°)}{E^\beta(c_p^*,\ 90°)}. \quad (5)$$

Recall that a similar correction approach is applied to all four polarization measurement combinations; however, for DoLP_p the corrections are additive, e.g.,

$$\mathrm{DoLP}_p(90°) = \mathrm{DoLP}_p^+(90°) + E^{\mathrm{DoLP}}(c_p^*,\ 90°). \quad (6)$$

E. Particulate Scattering and Backscattering Coefficients

To determine the particulate scattering and backscattering coefficients (b_p and b_{bp}) from the multiple-scattering-corrected β_p, an extrapolation procedure was used to provide data within the angular range 146°–180°. In brief, a factor κ was determined to estimate the contribution of scattering within the range 146°–180° to b_b by finding the best fit function to our measured total β within the angular range 90°–145° and then extrapolating the fit function to 180°. Note that we have altered

the procedure from our previous study [35] to find the best fit function of measured β with pure water included between 90° and 145°, rather than measured β_p between 90° and 150°, because it often results in a more realistic fitting of the functions describing scattering [76]. We then determined b_p and b_{bp} by subtracting theoretical pure seawater values of b_w and b_{bw} from total estimated b and b_b. Note that subscript "w" is used to indicate molecular scattering by pure water and dissolved salts determined using appropriate measurements of salinity and temperature described earlier. To avoid confusion in the Results sections, only multiple-scattering-corrected results are presented unless otherwise noted.

F. Statistical Analysis

Optical proxies for particulate characteristics were determined from a Model-I ordinary least-squares (OLS) linear regression analysis between optical (assumed here as the independent or explanatory variable) and particle mass concentration, size, or composition parameters (the dependent or response variables) measured on seawater samples described earlier. This approach is typically recommended for predictive relationships that seek to minimize error in the predicted (i.e., dependent) variable [77]. The determination of regression coefficients also utilized robust fitting of the data with a bisquare weighting function to limit the impact of outlier data [78]. Depending on the examined relationship, the linear, exponential, or power function was fitted to the data. To fit the exponential or power function, the data were subject to appropriate logarithmic transformation (using the logarithm to base e or 10) to linearize the fitted regression function.

In addition, we tested curve fitting to the data using a Model-II geometric mean (GM) regression analysis [79]. This approach was used in our previous analysis of San Diego samples [49]. Although for these samples the aggregate statistics characterizing the goodness of fit based on OLS and GM regressions were similar, GM provided generally somewhat better patterns of residuals between the model-predicted and measured values plotted as a function of measured values. In the current study, no clear advantage of GM was observed for such plots of residuals for combined dataset of San Diego and Prudhoe Bay samples, and for most examined relationships OLS regression models have improvements in nearly all aggregate statistical measures when compared with GM regressions. The OLS regression models for estimating the particulate characteristics from optical proxies were evaluated using several statistical metrics described in Table 1. These metrics were used to assess uncertainty of model-predicted values through comparison with observed values. Generally, we consider root-mean-square deviation (RMSD), median absolute percent difference (MdAPD), and median symmetric accuracy (MdSA) as measures of random error and median log-accuracy ratio (MdLQ) as a measure of bias. RMSD is a commonly used metric of random error based on average residuals between model-predicted and observed values. Whereas RMSD can be sensitive to outliers, MdAPD and MdSA utilize median operators and are accordingly less sensitive to extreme error. When computing MdAPD, underprediction is less heavily penalized than overprediction even if magnitude of error is the same, and therefore we also include MdSA [80,81]. In contrast to MdAPD, MdSA is not influenced by under- or overprediction because it is based on ratio values of predicted and observed values (Table 1). In terms of bias, we include MdLQ. This metric is similar to median ratio to describe under- and overprediction except that it is symmetric about a value of 0 so that negative values indicate systematic underprediction and positive values indicate systematic overprediction. Base-10 logarithms were used here so that a value of MdLQ $= 1$ means values are systematically overpredicted by an order of magnitude.

3. RESULTS AND DISCUSSION

The present study expands upon our recent work on light scattering proxies for particulate characterization. Our previous dataset consisted of data from primarily coastal waters of San Diego with light scattering measurements made in the laboratory with the LISST-VSF in benchtop mode [49]. In the current study, we include data from the turbid Arctic coastal waters near Prudhoe Bay with light scattering measurements made *in situ*. In these waters, the particulate beam attenuation coefficient c_p was in the range 0.4−22 m^{-1}, with over half of the measurements with $c_p > 5\ \mathrm{m}^{-1}$. These relatively high particle concentrations may influence our light scattering measurements; therefore, we begin by presenting results related to empirically developed corrections for the effects of multiple scattering and the impact of such corrections on our dataset. Next, we summarize particle characterization and light scattering measurements from field sampling around Prudhoe Bay. Finally, we describe results pertaining to optical proxies for predicting particulate characteristics associated with concentration, composition, and size distribution based on the combined Prudhoe Bay and San Diego datasets.

A. Multiple Scattering Corrections

Figure 3 depicts the final multiple scattering correction functions for β_p and DoLP_p, E^{β} and E^{DoLP}, respectively, as determined from the analysis described in Section 2.D. At $c_p^* = 20\ \mathrm{m}^{-1}$, β_p is nearly 3.5 times larger than it would be for the same particulate assemblage in a single scattering regime [Fig. 3(a)]. Only five of thirty-three Prudhoe Bay data points had measured c_p^* over 10 m^{-1}, and therefore emphasis is placed on results for $c_p^* < 10\ \mathrm{m}^{-1}$. For c_p^* in the range 2−10 m^{-1}, E^{β} values are 1–1.8 depending on scattering angle. The effects of multiple scattering for a given c_p^* are not constant with angle [Fig. 3(a)]. There are generally larger E^{β} values with increasing scattering angle as the path length of the LISST-VSF measurement geometry increases. For example, $E^{\beta}(c_p^* = 10\ \mathrm{m}^{-1}, \psi = 15°) = 1.58$, whereas $E^{\beta}(10\ \mathrm{m}^{-1}, 150°) = 1.77$. There are also differences in the ring detector's response to multiple scattering as compared with the eyeball sensor. The last several rings associated with $\psi > 10°$ have noticeably larger E^{β} when compared with the eyeball sensor angles near $\psi > 15°$ [Fig. 3(a)]. This is reasonable given that the acceptance angles are larger than 1° for these rings. E^{β} values decrease to a value of 1 for rings with smaller acceptance angles for $\psi < 1°$.

The E of the four polarized eyeball measurement combinations have similar patterns as E^{β}, except they are more impacted

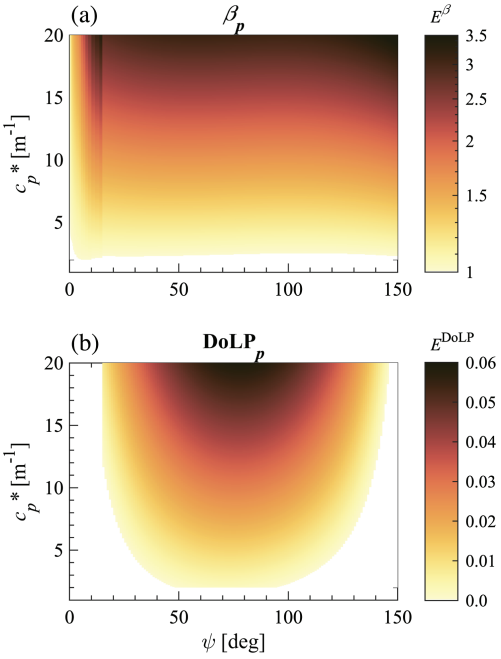

Fig. 3. Final multiple scattering correction functions E^β and E^{DoLP} for (a) β_p and (b) DoLP$_p$ as a function of scattering angle ψ and particulate beam attenuation coefficient with an adjustment for non-water absorption c_p^*. Color indicates value of E.

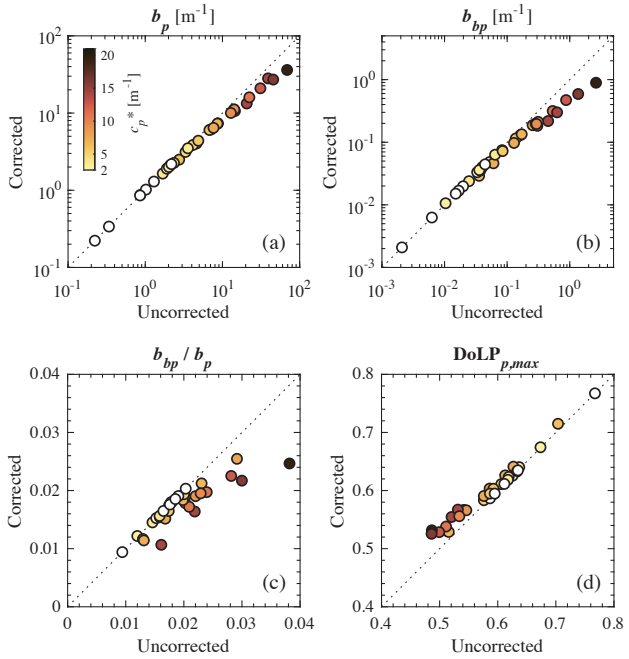

Fig. 4. Multiple-scattering-corrected versus uncorrected optical parameters from the Prudhoe Bay dataset. Data points are color filled by the non-water absorption-corrected value of particulate beam attenuation coefficient c_p^* as indicated in the color bar legend in (a). Unfilled data points have $c_p^* < 2$ m^{-1} and have no corrections applied. A 1:1 dotted line is shown for reference.

by unique angular features associated with minima near 90°, which are observed with these measurement combinations for natural assemblages of marine particles (not shown). The multiple scattering corrections for DoLP$_p$ are shown in Fig. 3(b). In contrast to E^β, corrections to DoLP$_p$ are minor for most angles except side-scattering angles with maximum values of E^{DoLP} found near $\psi = 80°$. At these angles, the measured DoLP$_p$ is at most 0.06 lower than expected because of multiple scattering when $c_p^* = 20$ m^{-1}. For c_p^* in the range 2−10 m^{-1}, E^{DoLP} at 90° ranges from 0 to 0.026.

The effects associated with multiple scattering are sensitive to scattering phase function, as well as other inherent polarization properties, in that subsequent scattering events will be dictated by the scattering properties of the particles. Ideally, multiple scattering corrections would be developed with particle assemblages from the water body of interest. However, when that is not feasible, the empirically-based multiple scattering corrections can be developed to approximate realistic particulate assemblages, which typically have strongly forward peaking scattering phase functions and a backscattering ratio ranging from about 0.005 to 0.025. We believe the particle assemblages used in the development of our multiple scattering correction functions are reasonable for approximating the multiple scattering effects of suspended particulate matter in the Arctic waters near Prudhoe Bay.

Corrected versus uncorrected values of four example optical parameters are presented in Fig. 4 to assess how the multiple scattering corrections impacted our dataset. First, we note that multiple scattering corrections were only applied to the twenty-five of thirty-three samples that had $c_p^* > 2$ m^{-1}, and, of these samples, c_p^* was 5%–25% lower than c_p. As expected, the largest values of b_p and b_{bp} experienced the largest reduction as a result of multiple scattering corrections, and we see divergence from the 1:1 line around and above the values of $b_p = 2$ m^{-1} and $b_{bp} = 0.3$ m^{-1} [Figs. 4(a), and 4(b)]. The reductions in b_p spanned from <1% to 50% with an average of 17%, while reductions in b_{bp} spanned <1% to 66% with an average of 26%. When considering the ratio b_{bp}/b_p, there was a decrease for nearly all samples with $c_p^* > 2$ m^{-1} because the multiple scattering corrections tended to be more substantial for b_{bp} [Fig. 4(c)]. On average, there was a 12% reduction in b_{bp}/b_p as a result of multiple scattering corrections. Unlike b_p or b_{bp}, the ratio b_{bp}/b_p showed no clear trend with uncorrected value; both low and high values of uncorrected b_{bp}/b_p experienced similar reductions after the multiple scattering corrections [Fig. 4(c)]. As expected, multiple scattering corrections resulted in an overall increase in the maximum value of DoLP$_p$ (DoLP$_{p,\mathrm{max}}$) because light becomes more randomly polarized following multiple scattering events [82,83]. On average, there was an increase of 3.2% in DoLP$_{p,\mathrm{max}}$ after multiple scattering corrections, and thus in comparison with other optical parameters shown in Fig. 4, multiple scattering corrections were relatively minor for DoLP$_{p,\mathrm{max}}$.

The results obtained using our multiple scattering corrections and shown in Fig. 4 are generally consistent with a recent study utilizing Monte Carlo radiative transfer simulations for the LISST-VSF instrument [60]. Ugulen *et al.* [60] found percent error of 100% for the LISST-VSF measured scattering coefficient of Arizona test dust sample as a result of multiple scattering when the sample optical thickness τ was 2. Using the multiple scattering corrections developed in the current study, we found percent error in b_p of about 100% for an optical thickness of

about 2.8. Thus, our corrections are reasonable and possibly conservative when compared with expected multiple-scattering error in LISST-VSF measurements based on the theoretical study by Ugulen *et al*. [60]. We recognize that multiple scattering is a probabilistic phenomenon and that multiple scattering effects may indeed be present for samples with c_p values around or below 2 m^{-1}. In our experimental work, we have found that dilution-corrected β_p are generally within 10% for c_p ranging from about 0.8 to 3.5 m^{-1}, with the higher values (i.e., $c_p > 1.8$ m^{-1}) being included in the present development of multiple scattering correction functions. In this development we did not include measurements with c_p below 1.8 m^{-1} primarily because of increased uncertainty in ring data from these samples.

B. Characterization of Prudhoe Bay Samples

Twelve locations were visited during two field campaigns near Prudhoe Bay late summer 2018 and 2019 (Fig. 1). Several locations were sampled multiple times, either days or a year later, providing 18 stations, which typically included two depths for optical and particulate characterization measurements. Example vertical profile data from optical and CTD instruments at three contrasting stations are shown in Fig. 5. Generally, there was fresher and warmer surface water on top of saltier and colder water [Figs. 5(a), 5(c), and 5(e)]. We expect this surface layer to be strongly influenced by river water given proximity to the Kuparuk, Sagavanirktok, Kadleroshilik, and Shaviovik Rivers (Fig. 1). Stations closest to shore also tended to have higher b_{bp} at the surface [Fig. 5(b)]. In terms of phytoplankton presence, we generally observed the depth of the maximum chlorophyll-a fluorescence deepening with distance further offshore [Figs. 5(b), 5(d), and 5(f)]. Although there were interesting features found at some stations in mid-depths associated with strong phytoplankton presence [e.g., K1b in Fig. 5(d)], we focused our efforts on the acquisition of prolonged time-series data with *in situ* optical instruments at surface and bottom depths because of a lack of real-time data. Nevertheless, a range of conditions can be found within our dataset of surface and bottom sampling, e.g., b_{bp} spanning 3 orders of magnitude and salinity ranging 10–30 PSU (Fig. 5).

Total mass concentration of suspended particulate matter (SPM) ranged from 0.6 g m^{-3} for UPE80 surface water to 32.2 g m^{-3} for N1b near-bottom water, and average SPM for the entire dataset was over 7 g m^{-3}. The total mass concentration of particulate organic carbon (POC) ranged from 70 to 540 mg m^{-3}. In terms of particulate composition, POC/SPM was 0.016–0.3 (on a g g^{-1} basis) with the average value less than 0.06, and only two samples contained particulate assemblages with POC/SPM > 0.12 (i.e., K1 and UPE80 surface). We interpret these findings as confirming the highly turbid and inorganic nature of particulate assemblages in this region. Although the particulate assemblages were predominately inorganic-dominated, the influence of phytoplankton in particulate assemblages was not negligible. For example, estimated chlorophyll-a concentrations (Chla) from *in situ* fluorometric measurements were 0.2−3.7 mg m^{-3} with the highest value observed in surface waters at NEWP1. The ratio of phytoplankton absorption to particulate absorption at 440 nm also ranged from 0.07 to 0.50 with nine samples containing values larger than 0.30.

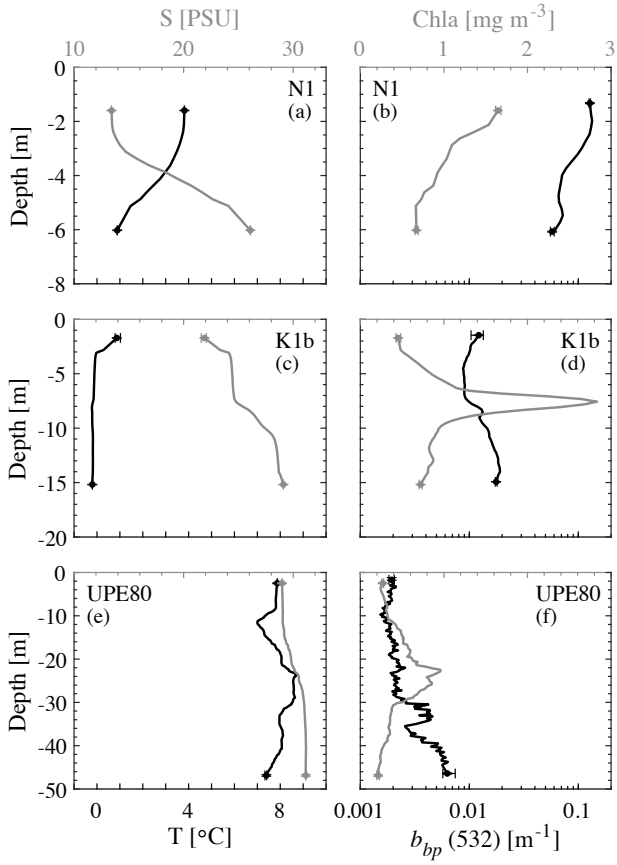

Fig. 5. Example vertical profile data at three stations (N1, K1b, and UPE80). Data have been median-binned within 0.25 m depth intervals. Depths corresponding to extended time-series acquisition of surface and bottom data are displayed with circles, and error bars represent the 25th and 75th percentile measurement data from the time-series measurements. Measurements of particulate backscattering coefficient are from a HydroScat-6 (HOBI Labs) instrument.

The estimated particle size distributions (PSDs) for the range of particle diameters D of 1 to 160 μm are shown in Fig. 6(a). The particle number concentrations spanned nearly 10 orders of magnitude over the size range 1–160 μm with maximum concentrations of 1 μm particles approaching 10^7 particles cm^{-3} at several stations. Recall that PSDs were determined by a method that inverts forward scattering measurements with 32 ring detectors based on Fraunhofer diffraction theory [30]. This approach results in a relatively coarse PSD with 32 size bins. Nonetheless, many of the PSDs did not appear to obey a Junge-type size distribution with a single slope of the log–log plot of PSD over the full size range. In particular, we see some noticeable variability within the larger particle sizes with $D > 20$ μm in Fig. 6.

We parameterized the PSDs in Fig. 6 using the 90th percentile particle diameter D_V^{90}, derived from the particle volume distribution [Fig. 6(b)]. Although PSD estimates are for the size range of 1–160 μm, we only utilized particle sizes between about 2 and 55 μm in the determination of D_V^{90} so that direct comparison with the San Diego dataset could be achieved. For the entire Prudhoe Bay dataset, D_V^{90} was 9–45 μm with only

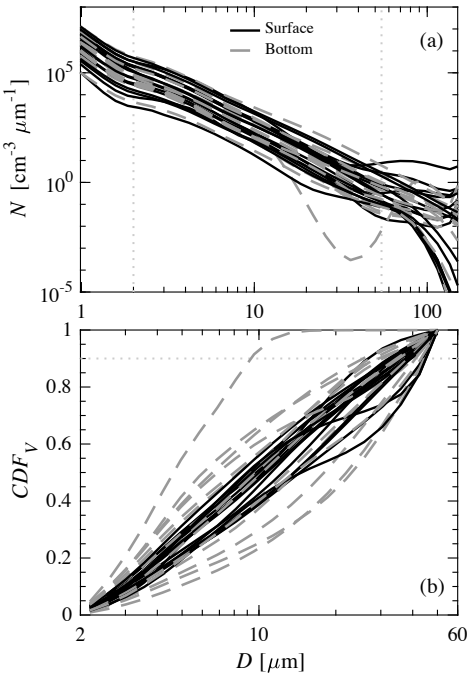

Fig. 6. Estimates of particle size distribution depicted as (a) number concentration and (b) cumulative distribution function of particle volume from LISST-VSF measurements of forward scattering by particles from Prudhoe Bay field sampling differentiated by depth of data acquisition. Particle diameter D represents midpoint of each size-bin. The dotted lines in (a) at particle diameters of 2 μm and 54.4 μm show the lower and upper cutoffs of the size range used for calculating D_V^{90}. The intersection of the horizontal dotted line in (b) and each CDF_V corresponds to D_V^{90}.

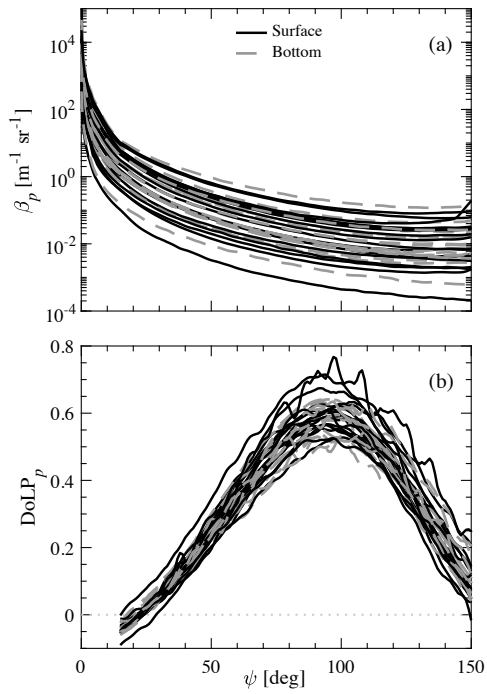

Fig. 7. LISST-VSF measurements of (a) β_p and (b) DoLP$_p$ from Prudhoe Bay field sampling differentiated by depth of data acquisition.

three samples exhibiting $D_V^{90} < 30$ μm, suggesting that particle assemblages generally contained significant proportions of large-sized particles [Fig. 6(b)].

C. Light Scattering by Particles in Waters near Prudhoe Bay

Results from measurements with the LISST-VSF at all stations are presented in Fig. 7. There was a large dynamic range seen within a single β_p spanning nearly 6 orders of magnitude for ψ in the range 0.08°–150° and nearly 3 orders of magnitude depending on scattering angle between β_p measured at different sampling locations [Fig. 7(a)]. There were no clear differences between all surface and all bottom measurements of β_p in terms of magnitude and angular shape; however, when considering most side and backwards scattering angles, the lowest β_p was measured in surface water at the offshore UPE80 station, and the highest β_p was measured in bottom water at the nearshore S1c station.

Figure 7(b) illustrates DoLP$_p$ as a function of scattering angle for all stations. The values of DoLP$_{p,\max}$ were 0.52–0.77 and were observed in the range of ψ between 89° and 106°. The larger angles of $\psi > 98°$ associated with DoLP$_{p,\max}$ have not been observed in our previous dataset from coastal San Diego waters [49], but they may be related to angular shifts of DoLP$_{p,\max}$ associated with particle composition [47,84,85]. In our previous study, we found the highest values of DoLP$_{p,\max}$ for particulate assemblages containing relatively higher proportions of small- versus large-sized particles, and we note that the three Arctic samples with the highest DoLP$_p$ values near 90° were from surface measurements [black lines in Fig. 7(b)]. We also found that DoLP$_p$ was negative for $\psi < 20°$ for nearly all samples, but it is unclear if this relates to measurement uncertainty or properties of the particulate assemblages given that at small angles DoLP$_p$ is expected to be small, eventually approaching zero at near-forward scattering angles (e.g., [86]). We acknowledge that some of the DoLP$_p$ data in Fig. 7(b) appear noisy, likely related to the low sampling rate of the LISST-VSF instrument, which resulted in about 40 measurements at some stations. Although we did find reasonable convergence to median values of DoLP$_p$(100°) for 30 to 60 measurements at many stations, we recommend closer to 100 measurements for *in situ* sampling to produce smoother DoLP$_p$ results.

D. Optical Proxies for Particle Mass Concentrations

We determined b_p and b_{bp} from β_p measurements presented in Fig. 7(a). Figure 8 depicts relationships between SPM and POC and the optical parameters c_p, b_p, and b_{bp}. All three optical coefficients (i.e., c_p, b_p, and b_{bp}) correlate strongly with SPM [Figs. 8(a)–8(c)]. The regression line for SPM versus b_{bp} in Fig. 8(c) resembles those previously reported by Reynolds *et al.* [20] in the Beaufort and Chukchi Seas. Similarity can also be seen in our regression line and a previously reported relationship between SPM and c_p from intensive sampling in coastal and offshore waters around Europe and French Guyana [18], although we acknowledge that the LISST instrument in the previous study utilized a laser with $\lambda = 660$ nm [Fig. 8(a)]. Generally, in the current study, the inorganic-dominated samples with the lowest POC/SPM have the highest c_p, b_p, and b_{bp} [Figs. 8(a)–8(c)].

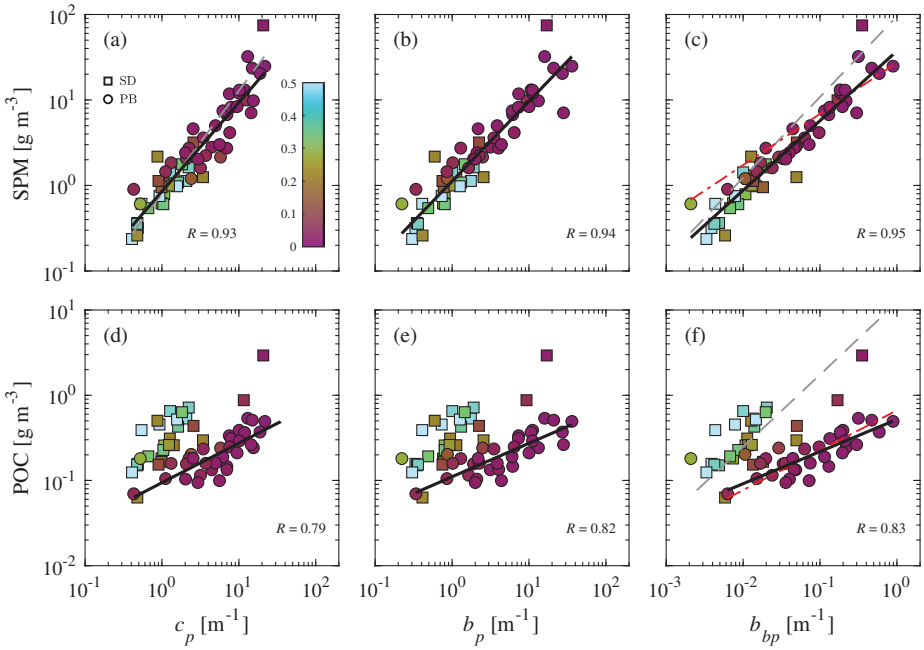

Fig. 8. (a)–(c) SPM and (d)–(f) POC as functions of c_p, b_p, and b_{bp} for San Diego (SD; squares) and Prudhoe Bay (PB; circles) samples. Data points are color filled by POC/SPM value as indicated in the color bar legend in (a). Dash-dotted and dashed lines in (c) and (f) are regression lines from Reynolds *et al*. [20] for $\lambda = 550$ nm (the gray dashed line is for all data, while the red dash-dotted line is for mineral-dominated particulate class only). The gray dashed line in (a) is from Neukermans *et al*. [18] ($\lambda = 660$ nm). Black lines represent linear regressions of $\log_{10}$-transformed data using all data in (a)–(c) and only PB data with POC/SPM < 0.12 in (d)–(f). Pearson correlation coefficient determined with $\log_{10}$-transformed data is displayed in each panel.

Table 2. Table of Best-Fit Regression Coefficients and Statistical Variables for Model Evaluation[a]

		Regression				*Model Evaluation*				
Optical Parameter	**Particle Parameter**	**Eq.**	***m***	***b***	***R***	**RMSD**	**MdAPD**	**MdSA**	**MdLQ**	***N***
c_p	SPM	Pow	1.039	0.853	0.93	7.9 g m^{-3}	28.3 %	36.8 %	–0.003	60
b_p	SPM	Pow	0.935	1.123	0.94	8.5 g m^{-3}	21.9 %	25.9 %	0.011	60
b_{bp}	SPM	Pow	0.815	37.31	0.95	8.2 g m^{-3}	18.7 %	20.3 %	0.016	60
c_p	POC	Pow	0.464	0.094	0.79	0.08 g m^{-3}	24.3 %	26.5 %	–0.023	31[b]
b_p	POC	Pow	0.393	0.110	0.82	0.08 g m^{-3}	26.2 %	29.9 %	–0.010	31[b]
b_{bp}	POC	Pow	0.377	0.519	0.83	0.07 g m^{-3}	21.8 %	24.3 %	0.004	31[b]
b_{bp}/b_p	POC/SPM	Exp	–217.52	3.092	–0.69	0.13	50.0 %	76.5 %	–0.010	58
b_{bp}/c_p	POC/SPM	Exp	–110.09	0.581	–0.76	0.14	50.3 %	94.0 %	–0.049	58
b_{bp}/b_p	$a_{ph}(440)/a_p(440)$	Exp	–92.26	1.027	–0.69	0.09	18.9 %	23.3 %	–0.019	46
b_{bp}/c_p	$a_{ph}(440)/a_p(440)$	Exp	–37.50	0.433	–0.54	0.11	30.5 %	42.5 %	0.010	46
$\beta_p^{\perp\parallel}(110°)/\beta_p^{\perp\perp}(18°)$	POC/SPM	Exp	–305.44	2.932	−0.89	0.07	36.8 %	39.4 %	−0.015	58
$\beta_p^{\perp\parallel}(110°)/\beta_p^{\perp\perp}(18°)$	POC/SPM	Pow	−3.124	6.598×10^{-8}	−0.91	0.09	29.8 %	37.6 %	−0.001	58
$\mathrm{DoLP}_{p,\max}$	POC/SPM	Exp	9.784	1.172×10^{-4}	0.85	0.01	19.3 %	23.4 %	0.029	31[c]
$\mathrm{DoLP}_{p,\max}$	D_V^{90}	Lin	−91.14	87.86	−0.78	6.2 µm	13.2 %	14.5 %	−0.006	71

[a]Models are the optically-based relationships for estimating particle parameters that characterize particulate assemblages in terms of mass concentration, size, or composition. Optical parameters are independent variables (x), and particle parameters are dependent variables (y). Linear (Lin) equations are of the form $y = mx + b$, exponential (Exp) equations are of the form $y = be^{mx}$, and power (Pow) equations are of the form $y = bx^m$. For the exponential relationships, the correlation coefficient R was determined using log-transformed values of particle parameter and untransformed values of optical parameter, while for power relationships R was determined using $\log_{10}$-transformed optical and particle parameters. Regressions were developed and model performances were evaluated using all San Diego and Prudhoe Bay data, excluding outliers, unless otherwise noted. All regressions are significant (F-test, $p < 10^{-5}$).

[b]Regression and model performance use only Prudhoe Bay data with POC/SPM < 0.12.

[c]Regression and model performance use all data with POC/SPM < 0.12.

Table 2 includes regression coefficients and statistical parameters to evaluate models shown in Fig. 8. When compared with c_p and b_p, b_{bp} appears as the more effective optical proxy for SPM. This can be seen in Figs. 8(a)–8(c) where data points have a tighter spread around the regression line in Fig. 8(c). This is also supported in Table 2 with statistical parameters representing median error: MdAPD and MdSA. The predictive relationship for SPM based on b_{bp} has MdAPD and MdSA less than about

20%. In terms of MdAPD and MdSA, the b_p regression model is less accurate and c_p model is least accurate (Table 2). We acknowledge here that the measure of bias (i.e., MdLQ) suggests there is some systematic overprediction of SPM in the b_{bp} model, while the c_p model has the least bias (Table 2). Similar findings have been observed regarding improved relationships between b_{bp} and SPM compared with c_p and SPM [18,87], although to our knowledge no previous analyses relied on estimates of b_p and b_{bp} from integration of measured β_p over a wide angular range.

When it comes to proxies for POC based on c_p, b_p, and b_{bp} measurements, a single robust relationship breaks down, which can be attributed primarily to variations in composition of particulate assemblages [Figs. 8(d)–8(f)]. Similar results were found in Reynolds *et al*. [20], and there is good agreement between most of the Prudhoe Bay data and the inorganic-dominated trend line from their study [Fig. 8(f)]. A composition-specific regression model for POC emerges with uncertainty of around 20%–30%, depending on the optical proxy, for inorganic-dominated assemblages (POC/SPM < 0.12) of the Prudhoe Bay data (Table 2). In this case, b_{bp} appears as the most effective proxy for POC with the lowest MdAPD and MdSA, followed by c_p and then b_p (Table 2). It is important to recognize that the results of this analysis naturally depend on the assumed value of the POC/SPM cutoff for inorganic-dominated particulate assemblages. While the assumption of POC/SPM < 0.12 seems reasonable, a more conservative (i.e., lower) cutoff value could be used [42]. In general, however, the usefulness of POC/SPM data to classify particulate matter into inorganic-dominated, organic-dominated, and mixed assemblages for subsequent formulation of regression models to estimate POC from optical measurements was demonstrated before [20,42].

E. Optical Proxies for Advanced Particle Characterization

In Figs. 9–11, we plot various measures describing particle composition and size distribution as functions of several optical proxies. When linear correlations are strong (which we assume as having $|R| > 0.60$), regression lines are plotted; one using only San Diego data (gray dash-dotted line) and the other using our entire dataset of Prudhoe Bay and San Diego data (black solid line). Note that log-transformed data are utilized in most regression and correlation analyses as indicated in subsequent figures and table. Consistency between the two regression lines suggests a relationship that is relatively independent of location of coastal environment. We evaluate the regression models using the entire dataset of Prudhoe Bay and San Diego data. Two or three data points from Prudhoe Bay are identified in the figures that are not included in the regression and validation analysis. These data are excluded from regression-model development because they represent extremes in the data or have higher uncertainties regarding measurement quality.

First, we evaluate a commonly cited proxy for particle composition: the ratio of b_{bp}/b_p, also referred to as the particulate backscattering ratio, which does not include polarization information. In modeling simulations of homogenous spherical particles, this proxy is sensitive to refractive index of particles; however, it still includes some effects of particle size [29].

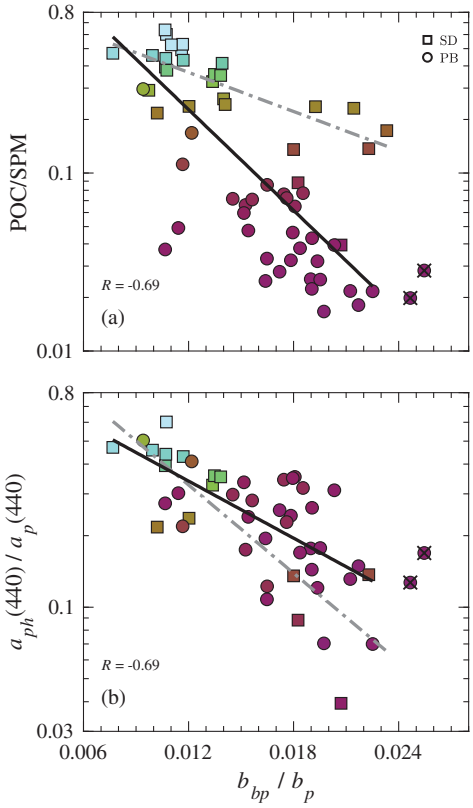

Fig. 9. Particle composition parameters (a) POC/SPM and (b) $a_{ph}(440)/a_p(440)$ as a function of b_{bp}/b_p for San Diego (SD; squares) and Prudhoe Bay (PB; circles) samples. Data points are color filled by POC/SPM value as indicated in the color bar legend of Fig. 8(a). Linear regressions using all data and only SD data are shown with a black line and gray dash-dotted line, respectively. Linear regressions were determined using $\log_e$-transformed particle composition data, and Pearson correlation coefficient based on all data is displayed in each panel. Data not included in regression analysis are marked with a "X."

Typically, *in situ* measurements of b_{bp}/b_p reported in the literature rely on indirect determinations of b_p from instruments measuring non-water absorption and beam attenuation, and they are prone to scattering errors in some cases [88]. *In situ* determinations of b_{bp} have typically relied on scattering measurements at a single or a few backward angles only (e.g., [89]). Our measurements of both b_p and b_{bp} are more direct in the sense that the volume scattering function β_p was measured over the angular range of 0.08°–145° and extrapolated to 180° for integration of β_p over appropriate angular ranges to estimate b_p and b_{bp}.

Figure 9 depicts the two parameters describing particle composition as a function of b_{bp}/b_p. The ratio $a_{ph}(440)/a_p(440)$ can be considered to be generally representative of the relative proportions of phytoplankton versus non-phytoplankton particles, while the assessment of composition with POC/SPM provides a proxy of the contribution of all organic material to SPM, whether it be phytoplankton or non-phytoplankton particles. Whereas $a_{ph}(440)/a_p(440)$ can theoretically achieve values of 1 for a sample that is entirely dominated by phytoplankton, values of POC/SPM tend to approach maximum values between about 0.4 and 0.55 in the ocean [39,90–92], and

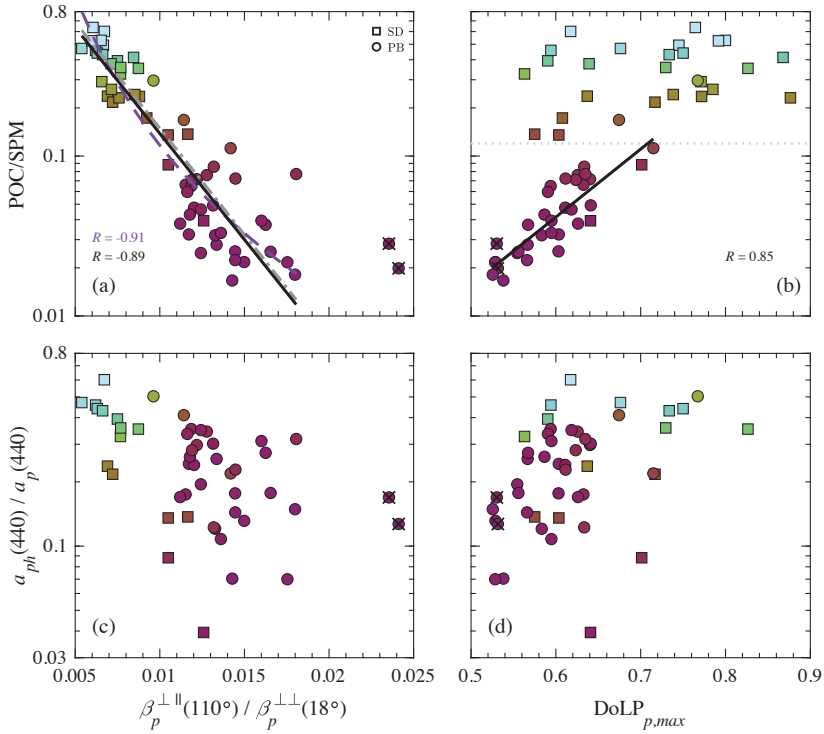

Fig. 10. Particle composition parameters (a),(b) POC/SPM and (c),(d) $a_{ph}(440)/a_p(440)$ as functions of (a),(c) $\beta_p^{\perp\parallel}(110°)/\beta_p^{\perp\perp}(18°)$ and (b),(d) $DoLP_{p,max}$ for San Diego (SD; squares) and Prudhoe Bay (PB; circles) samples. Data points are color filled by POC/SPM value as indicated in the color bar legend of Fig. 8(a). Linear regressions using all data and only SD data are shown with a black line and gray dash-dotted line, respectively. Linear regressions were determined using $\log_e$-transformed particle composition data and Pearson correlation coefficient based on all data is displayed in each panel if value exceeds 0.60. An additional regression line in (a) is shown with a purple dashed line and was determined with $\log_{10}$-transformed data. Outliers not included in regression analysis are displayed with a "X." The regression line in (b) only utilizes data with POC/SPM < 0.12.

only two samples with values over 0.55 are observed in the current study. The values of POC/SPM from the current study are in the approximate range 0.02–0.64, while $a_{ph}(440)/a_p(440)$ ranges from less than 0.04 up to 0.60. With the combination of the Prudhoe Bay and San Diego datasets, POC/SPM values range nearly three orders of magnitude, with the Prudhoe Bay data complementing the San Diego dataset that included mostly relatively high POC/SPM with only two measurements of POC/SPM < 0.14 [Fig. 9(b)]. The values of b_{bp}/b_p are in the approximate range 0.007–0.026, which is consistent with data from other studies [32,34,37,93]. In general, lower values of b_{bp}/b_p tend to be observed with increasing contribution of phytoplankton to particulate absorption or increasing POC/SPM, and the highest values of b_{bp}/b_p are found for non-phytoplankton-dominated assemblages regardless of whether contributions of inorganic matter or contributions of non-algal particles are significant (Fig. 9).

In Fig. 9, the two Prudhoe Bay data points which represent the highest values of the particulate backscattering ratio (i.e., $b_{bp}/b_p > 0.024$) are marked with an "X" and not included in the analyses of optical proxies for particle composition. There is a noticeable difference between the San Diego and all data trend lines for POC/SPM versus b_{bp}/b_p [Fig. 9(a)]. This is mostly driven by the cluster of four data points with POC/SPM = 0.014−0.24 and high particulate backscattering ratio ($b_{bp}/b_p > 0.02$). These particulate assemblages are all from the San Diego River Estuary, and three of the four samples are 5 μm filtrates [49]. It is possible these samples contain appreciable scattering contributions from small or submicrometer mineral particles, which could increase b_{bp}/b_p. On the other hand, San Diego and all data trend lines for $a_{ph}(440)/a_p(440)$ versus b_{bp}/b_p are relatively similar [Fig. 9(b)]. Therefore, the predictive capabilities of b_{bp}/b_p may perhaps be limited to distinguishing phytoplankton dominated from non-phytoplankton-dominated assemblages (see also [31]). Table 2 includes the model evaluation of the regression analysis based on all data points and validates the assessment that b_{bp}/b_p is a more effective proxy for $a_{ph}(440)/a_p(440)$ than for POC/SPM. For example, MdAPD and MdSA are over twice as low for estimations of $a_{ph}(440)/a_p(440)$ compared with estimations of POC/SPM based on b_{bp}/b_p. We briefly mention here that within our data, no improvements were observed for the optical proxy b_{bp}/c_p compared with b_{bp}/b_p as an estimator of $a_{ph}(440)/a_p(440)$ or POC/SPM (Table 2).

Figure 10 illustrates particle composition parameters as functions of polarized light scattering metrics. In Koestner *et al.* [49], an optical proxy for particle composition was suggested after identifying the polarization measurement combination at two scattering angles which best predicted POC/SPM and also appeared to be weakly sensitive to a particle size parameter. The measurement combination was $\beta_p^{\perp\parallel}(110°)/\beta_p^{\perp\perp}(18°)$, where the first and second superscript characters denote the incident and detected polarization states of the LISST-VSF instrument, respectively. Note that an inadvertent error was

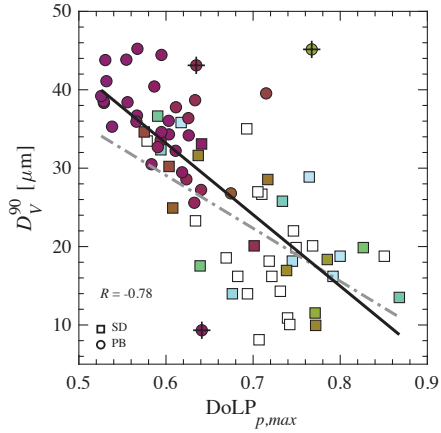

Fig. 11. Particle size parameter D_V^{90} as a function of DoLP$_{p,\max}$ for San Diego (SD; squares) and Prudhoe Bay (PB; circles) samples. Data points are color filled by POC/SPM value as indicated in the color bar legend of Fig. 8(a). Unfilled SD data points have no POC/SPM data. Linear regressions using all data and only SD data are shown with a black line and gray dash-dotted line, respectively. Pearson correlation coefficient for all data is displayed. Outliers not included in regression analysis are displayed with a "+".

made in the presentation of results in the previous publication [49], which mistakenly referred to parallel as perpendicular and vice versa. An erratum was published to address this issue [94]. In the present analysis we include the mostly turbid and inorganic-dominated Prudhoe Bay data to assess potentially broader applicability of the polarization-based proxy that was originally identified from only San Diego data.

The proxy $\beta_p^{\perp\parallel}(110°)/\beta_p^{\perp\perp}(18°)$ has a strong linear correlation with POC/SPM with most data points falling along the trend lines in Fig. 10(a). Furthermore, the trend line based on San Diego data appears very similar to trend lines using all data [Fig. 10(a)]. This is in stark contrast to the regression model for POC/SPM based on b_{bp}/b_p, which had a larger spread of data around the trend lines and differences between trend lines [Fig. 9(a)]. Unlike the backscattering ratio, $\beta_p^{\perp\parallel}(110°)/\beta_p^{\perp\perp}(18°)$ does not have a strong linear correlation with $a_{ph}(440)/a_p(440)$ for the entire combined dataset [Fig. 10(c)], so trend lines are not shown ($R = -0.50$). Although the San Diego data show a strong trend of decreasing value of $\beta_p^{\perp\parallel}(110°)/\beta_p^{\perp\perp}(18°)$ with increasing contribution of phytoplankton to particulate absorption ($R = -0.89$), the Prudhoe Bay data alone have weak correlation because of significant scatter [Fig. 10(c)].

The improvements of $\beta_p^{\perp\parallel}(110°)/\beta_p^{\perp\perp}(18°)$ compared with b_{bp}/b_p as a proxy for particle composition parameter POC/SPM can also be seen in terms of statistical metrics assessing the models (Table 2). For example, MdSA is lower by nearly a factor of 2 for estimations of POC/SPM from $\beta_p^{\perp\parallel}(110°)/\beta_p^{\perp\perp}(18°)$ compared with estimations from b_{bp}/b_p (Table 2). Some of the highest $\beta_p^{\perp\parallel}(110°)/\beta_p^{\perp\perp}(18°)$ values from Prudhoe Bay do tend to skew the best fit regression line to a slight systematic underprediction of high POC/SPM values [Fig. 10(a)]. An additional power model using $\log_{10}$-transformed optical and particle parameters appears to provide improvements in bias and random error with accuracy of about 30%–38% (assessed with MdAPD and MdSA), although RMSD, which is more sensitive to large errors, is marginally worse for this power model (Table 2). Although $\beta_p^{\perp\parallel}(110°)/\beta_p^{\perp\perp}(18°)$ as a proxy for POC/SPM was originally identified through empirical analysis of measurements, physical interpretation is possible through algebraic manipulation of equations in Table 1. The polarized light scattering proxy $\beta_p^{\perp\parallel}(110°)/\beta_p^{\perp\perp}(18°)$ is approximately proportional to $\frac{\beta_p(110°)}{\beta_p(18°)} \times \frac{\mathrm{DoLP}_p(110°)+P_{22}(110°)}{P_{22}(18°)}$, where P_{22} is the matrix element p_{22} normalized by p_{11}. The polarized light scattering proxy is therefore related to the unpolarized ratio $\beta_p(110°)/\beta_p(18°)$, which is expected to behave similarly to the particulate backscattering ratio b_{bp}/b_p; however, this polarized light scattering proxy includes some weighting based on polarization properties such as DoLP$_p$ near its maximum value and P_{22} at 110° and 18°. In our previous study, we found that DoLP$_{p,\max}$ and $P_{22}(100°)$ were reasonably good proxies for particle size parameters and had weak correlation with particle composition parameters, while $P_{22}(20°)$ was a reasonably good proxy for particle composition parameters and had weak correlation with particle size parameters [49]. Thus, it is possible to interpret $\beta_p^{\perp\parallel}(110°)/\beta_p^{\perp\perp}(18°)$ as potentially accounting for additional effects of particle size distribution on light scattering, which may not be explicitly accounted for in $\beta_p(110°)/\beta_p(18°)$ or b_{bp}/b_p. We briefly note here that, as also seen in our previous study, $\beta_p(110°)/\beta_p(18°)$ underperformed $\beta_p^{\perp\parallel}(110°)/\beta_p^{\perp\perp}(18°)$ as a proxy for composition parameters POC/SPM and $a_{ph}(440)/a_p(440)$ in terms of all statistical metrics examined.

In Fig. 10 we also present particle compositional parameters as functions of DoLP$_{p,\max}$. Although a strong linear correlation was not observed between particle composition parameters and DoLP$_{p,\max}$ with only San Diego data [49], various studies suggest DoLP$_{p,\max}$ can be sensitive to particle composition [47,84,85]. A strong linear correlation is not observed between $a_{ph}(440)/a_p(440)$ and DoLP$_{p,\max}$ for the entire dataset [$R = 0.39$; Fig. 10(d)]; however, a pattern emerges for a relationship between POC/SPM and DoLP$_{p,\max}$ when POC/SPM is low [Fig. 10(b)]. When considering only the inorganic-dominated assemblages (i.e., data points with POC/SPM < 0.12), there is a strong linear correlation between POC/SPM and DoLP$_{p,\max}$ ($R = 0.85$). Model estimations seem quite good for DoLP$_{p,\max}$ as a proxy for POC/SPM (Table 2), but only when this inorganic-dominated condition is met within our data. It is clear that DoLP$_{p,\max}$ varies significantly for similar POC/SPM values when particulate assemblages are not inorganic-dominated, i.e., with POC/SPM > 0.12 [Fig. 10(b)]. For example, nearly the entire range of DoLP$_{p,\max}$ 0.59–0.87 is seen for POC/SPM of approximately 0.40 [Fig. 10(b)]. For the cases of POC/SPM > 0.12, which can be assumed as mixed or organic-dominated, other properties of particles must be responsible for such variability.

In Koestner *et al.* [49], we found that DoLP$_{p,\max}$ was strongly correlated with particle size parameter D_V^{90} for the San Diego dataset. Figure 11 presents D_V^{90} as a function of DoLP$_{p,\max}$ for all Prudhoe Bay and San Diego data. The inclusion of the Prudhoe Bay data expands the San Diego dataset with larger

D_V^{90} values greater than 30 μm. Note that three data points in Fig. 11 are marked with a "+" and excluded from regression analysis because of increased uncertainty in measurements with the LISST-VSF ring detectors for these samples. The trend line developed with only San Diego data is similar to the trend line developed with all data (Fig. 11). Thus, the relationship between particle size parameter D_V^{90} and $\mathrm{DoLP}_{p,\max}$ observed within the entire dataset does not appear to be region specific. Remarkably, aggregate statistical metrics suggest there is minimal bias and accuracy of better than 15% for estimating D_V^{90} from $\mathrm{DoLP}_{p,\max}$ using the linear model shown in Fig. 11 (Table 2).

We provide some additional comments here regarding our particle size distribution measurements. We acknowledge that the particle sizing approach for the Prudhoe Bay samples was different than the impedance-based particle counting technique utilized with San Diego samples [35,49]. However, the two approaches can provide good agreement over the particle size range of about 1 to 50 μm for broad polydisperse assemblages [69]. Additional comparison experiments using seawater samples from San Diego coastal waters were performed to assess similarity of PSDs using the Multisizer 3 (Beckman Coulter) and the LISST-VSF diffraction-based approach. Of most relevance to the current study, D_V^{90} values were less than 10% higher based on LISST-VSF measurements as compared with Multisizer 3 measurements.

Although $\mathrm{DoLP}_{p,\max}$ does trend with POC/SPM for low POC/SPM values, it is unclear if particle size is driving this relationship, because as can be seen in Fig. 12, the majority of the low POC/SPM data also have high D_V^{90} values. We suspect this may be related to aggregation facilitated by terrestrial material deposited by various river systems in the Prudhoe Bay region (Fig. 1). Quantitatively, there are improvements in MdAPD and MdSA of $\mathrm{DoLP}_{p,\max}$-based estimations of D_V^{90} (about 14%) compared with estimations of POC/SPM (about 21%), even when only utilizing the low POC/SPM data in evaluating the latter estimations (Table 2). Additionally, if only data points which include both D_V^{90} and POC/SPM measurements are compared, there are improvements in the statistical significance

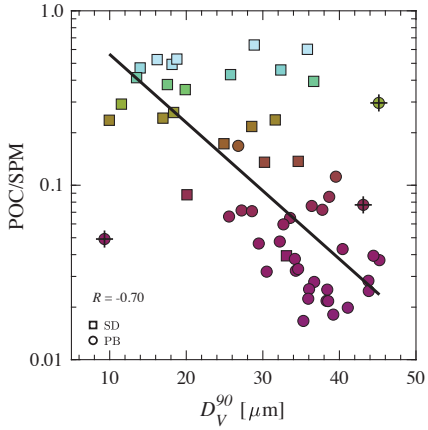

Fig. 12. POC/SPM as a function of D_V^{90} for San Diego (SD; squares) and Prudhoe Bay (PB; circles) samples. Data points are colored by POC/SPM value as indicated in the color bar legend of Fig. 8(a). Linear regression using all data is shown with a black line. Pearson correlation coefficient is displayed. Data not included in regression analysis are marked with a "+".

(i.e., null hypothesis p-value) by over 5 orders of magnitude for D_V^{90} versus $\mathrm{DoLP}_{p,\max}$ compared to POC/SPM versus $\mathrm{DoLP}_{p,\max}$ (not shown). To more confidently conclude the differing roles of particle size distribution and composition in $\mathrm{DoLP}_{p,\max}$ for natural assemblages of aquatic particles, more measurements in other regions are needed, especially with samples containing predominantly small-sized particles that are inorganic and predominantly large-sized particles that are organic.

4. SUMMARY AND CONCLUDING REMARKS

The current study expands upon our previous work regarding the development of optical proxies based on angle-resolved light scattering measurements to estimate particle size and compositional characteristics of natural assemblages of aquatic particles. These optical proxies can be useful for potential application of optical measurements from autonomous platforms, moorings, and traditional ship-based operations. While the previous studies [35,49] involved evaluation of highly contrasting natural assemblages of particles from San Diego coastal environments, the current study includes samples from Arctic coastal waters that are representative of more turbid and inorganic-particle dominated waters with influence of terrestrial material. Comprehensive analysis of these new samples involved *in situ* measurements of angle-resolved polarized light scattering and characterization of particulate material with various parameters derived from particle mass concentration, particulate organic carbon concentration, particle size distribution, and particulate light absorption measurements.

We first developed empirical corrections for undesired effects of multiple scattering, which can impact light scattering measurements in highly turbid environments. These corrections enable effective *in situ* use of the LISST-VSF instrument in various aquatic environments, including relatively turbid waters when the particulate beam attenuation coefficient exceeds $2\ \mathrm{m}^{-1}$. Second, we presented measurement results of angular distribution of polarized light scattered by particles in Arctic coastal waters with concurrent measurements of particulate properties associated with particulate composition and size distribution. Finally, we evaluated various optical measurements as proxies for SPM and POC, as well as particle composition and size distribution parameters.

The current study demonstrates that the particulate backscattering coefficient b_{bp} is a more effective predictor of SPM as compared with the particulate scattering coefficient b_p and particulate beam attenuation coefficient c_p. All three optical measurements are generally weak proxies for POC unless particulate assemblages are classified beforehand in terms of particle composition based on proportions of organic and inorganic matter in SPM as parameterized by the POC/SPM ratio. The ratio of $\beta_p^{\perp\parallel}(110°)/\beta_p^{\perp\perp}(18°)$ is an effective proxy for particle composition parameter POC/SPM over a wide range of assemblages of aquatic particles from coastal waters in Southern California and Northern Alaska, while the ratios b_{bp}/b_p or b_{bp}/c_p are not nearly as effective. In terms of estimating a particle size parameter, $\mathrm{DoLP}_{p,\max}$ is a reasonably good proxy for D_V^{90} for our entire dataset, achieving less than 15% uncertainty. Note that an additional proxy for D_V^{90}, i.e., $\beta_p^{\perp\parallel}(110°)/\beta_p^{\perp\perp}(110°)$,

was also evaluated but did not perform satisfactorily when the examined dataset included the data from Prudhoe Bay. The optical proxies $\beta_p^{\perp\parallel}(110°)/\beta_p^{\perp\perp}(18°)$ and $\mathrm{DoLP}_{p,\max}$ for particle composition and size parameters, respectively, showed no appreciable differences in their predictive capabilities between the examined datasets from the two contrasting coastal marine environments in the Southern California and Northern Alaska regions.

$\mathrm{DoLP}_{p,\max}$ values were found to be approximately 0.5–0.9 for a wide range of natural particle assemblages examined. Although $\mathrm{DoLP}_{p,\max}$ was strongly correlated with particle size, it is unclear from our dataset what role particle composition may play in driving changes of $\mathrm{DoLP}_{p,\max}$. In our data, when samples are organic-dominated (phytoplankton or non-phytoplankton), particle size is clearly an important driver of change in $\mathrm{DoLP}_{p,\max}$, whereas particle composition does not appear to have any clear influence on $\mathrm{DoLP}_{p,\max}$. On the other hand, when particle assemblages are inorganic-dominated, composition appears to be relevant in that there is a trend of decreasing values of $\mathrm{DoLP}_{p,\max}$ coinciding with decreasing POC/SPM which is indicative of increasing contribution of inorganic particles. The roles of size and composition cannot, however, be separated because overall there is a trend of increasing D_V^{90} with decreasing POC/SPM within our dataset. Such trends can be variable across diverse marine environments; for example, in another study of near-shore waters at San Diego's Imperial Beach, opposite trends between D_V^{90} and POC/SPM were observed [42]. Further studies encompassing even more diverse environments and particulate assemblages, specifically assemblages containing a high abundance of small-sized inorganic particles, are required to improve the assessment of the relationships between $\mathrm{DoLP}_{p,\max}$ and particle properties that have been observed in the current study.

The consequences of rapidly changing Arctic environments are expected to be clearly manifested in coastal regions such as the region near Prudhoe Bay [95,96]. To our knowledge, we presented the first comprehensive characterization of angle-resolved polarized light scattering properties of aquatic particle assemblages in Arctic coastal waters while also explaining the variability of measured optical properties in terms of measured particle size and compositional parameters. Given the remote nature of the Arctic region and anticipated future changes in the Arctic marine environments including dynamics of suspended biological and non-biological particulate matter, we expect the results of the present study can be particularly useful for advancing the potential applicability of optical measurements from *in situ* platforms such as autonomous floats and moorings as well as from above-water remote sensing radiometric and polarimetric sensors. Furthermore, there is a need for the advancement of optically-based approaches for deriving biogeochemically relevant parameters linked to primary production and the biological carbon pump (e.g., [97,98]), and we believe findings from the current study can inform the development of new polarized light scattering sensors for use on autonomous platforms in the ocean such as biogeochemical Argo floats [2] and gliders.

Funding. National Aeronautics and Space Administration (NNX17AI72G).

Acknowledgment. This study was initiated and conducted largely when the first author (D.K.) was with the Scripps Institution of Oceanography, University of California San Diego. Part of this research was performed while D.K. held an NRC Research Associateship award at the Naval Research Laboratory. We express our appreciation to Krista Longnecker, Luka Catipovic, Ryan O'Shea, Samuel Laney, and Stephen Okkonen for assistance during field data collection and special thanks to Luka Catipovic for processing of CTD, ac-s, and ECO-Triplet data. Additional thanks to Captain Mike Fleming of the R/V Ukpik, to Jack Pan and Kiefer Forsch for providing glacial meltwater sample, and to Ishan Joshi for support during particulate absorption measurements. We also express our gratitude to Wesley Moses and Stephen Okkonen for assistance in creating Fig. 1. POC analysis of seawater samples was done at the Marine Science Institute, University of California Santa Barbara. We thank two anonymous reviewers for their constructive comments.

Disclosures. The authors declare no conflicts of interest.

Data Availability. Data from the current study have yet to be made publicly available but are available upon request.

REFERENCES

1. D. Antoine, M. Chami, H. Claustre, F. d'Ortenzio, A. Morel, G. Bécu, B. Gentilli, F. Louis, J. Ras, E. Roussier, A. J. Scott, D. Tailliez, S. B. Hooker, P. Guevel, J. F. Desté, and D. Adams, "BOUSSOLE: a joint CNRS-INSU, ESA, CNES, and NASA ocean color calibration and validation activity," National Aeronautics and Space Administration Technical Memorandum No. 2006-214147 (2006).
2. Biogeochemical-Argo Planning Group, *The Scientific Rationale, Design and Implementation Plan for a Biogeochemical-Argo Float Array*, K. Johnson and H. Claustre, eds. (2016).
3. T. D. Dickey and G. C. Chang, "Recent advances and future visions: temporal variability of optical and bio-optical properties of the ocean," Oceanography **14**, 15–29 (2001).
4. K. Niewiadomska, H. Claustre, L. Prieur, and F. d'Ortenzio, "Submesoscale physical-biogeochemical coupling across the Ligurian current (Northwestern Mediterranean) using a bio-optical glider," Limnol. Oceanogr. **53**, 2210–2225 (2008).
5. C. M. Yentsch and C. S. Yentsch, "Emergence of optical instrumentation for measuring biological properties," in *Oceanogr. Mar. Biol.* H. Barnes and M. Barnes, eds. **22** (Aberdeen University Press,, 1984) pp. 55–98.
6. E. B. Barbier, S. D. Hacker, C. Kennedy, E. W. Koch, A. C. Stier, and B. R. Silliman, "The value of estuarine and coastal ecosystem services," Ecol. Monographs **81**, 169–193 (2011).
7. N. Greenwood, E. R. Parker, L. Fernand, D. B. Sivyer, K. Weston, S. J. Painting, S. Kröger, R. M. Forster, H. E. Lees, D. K. Mills, and R. W. P. M. Laane, "Detection of low bottom water oxygen concentrations in the North Sea; implications for monitoring and assessment of ecosystem health," Biogeosciences **7**, 1357–1373 (2010).
8. S.-W. Lee, G. Park, and K.-H. Choi, "Biomass of plankton and macrobenthos and benthic species diversity in relation to environmental gradients in a nationwide coastal survey," Regional Stud. Mar. Sci. **26**, 100502 (2019).
9. A. Morel, "Diffusion de la lumière par les eaux de mer: Resultats expérimentaux et approche théorique," in *Optics of the Sea*, AGARD lecture series (North Atlantic Treaty Organization, 1973), Vol. **61**, pp. 3.1.1–3.1.76.
10. C. D. Mobley, *Light and Water: Radiative Transfer in Natural Waters* (Academic, 1994).
11. M. Babin, D. Stramski, G. M. Ferrari, H. Claustre, A. Bricaud, G. Obolensky, and N. Hoepffner, "Variations in the light absorption coefficients of phytoplankton, nonalgal particles, and dissolved organic matter in coastal waters around Europe," J. Geophys. Res. Oceans **108**, 3211 (2003).
12. D. Stramski, E. Boss, D. Bogucki, and K. J. Voss, "The role of seawater constituents in light backscattering in the ocean," Prog. Oceanography **61**, 27–56 (2004).
13. V. Vantrepotte, H. Loisel, D. Dessailly, and X. Mériaux, "Optical classification of contrasted coastal waters," Remote Sens. Environ. **123**, 306–323 (2012).

14. A. D. McGuire, L. G. Anderson, T. R. Christensen, S. Dallimore, L. Guo, D. J. Hayes, M. Heimann, T. D. Lorenson, R. W. Macdonald, and N. Roulet, "Sensitivity of the carbon cycle in the Arctic to climate change," Ecol. Monographs **79**, 523–555 (2009).
15. B. C. McMeans, N. Rooney, M. T. Arts, and A. T. Fisk, "Food web structure of a coastal Arctic marine ecosystem and implications for stability," Mar. Ecol. Prog. Ser. **482**, 17–28 (2013).
16. M. Jonasz and G. Fournier, *Light Scattering by Particles in Water: Theoretical and Experimental Foundations* (Elsevier, 2007).
17. J. P. Downing, R. W. Sternberg, and C. R. B. Lister, "New instrument for the investigation of sediment suspension processes in the shallow marine environment," Mar. Geol. **42**, 19–34 (1981).
18. G. Neukermans, H. Loisel, X. Meriaux, R. Astoreca, and D. McKee, "In situ variability of mass-specific beam attenuation and backscattering of marine particles with respect to particle size, density, and composition," Limnol. Oceanogr. **57**, 124–144 (2012).
19. A. Poteau, E. Boss, and H. Claustre, "Particulate concentration and seasonal dynamics in the mesopelagic ocean based on the backscattering coefficient measured with biogeochemical-argo floats," Geophys. Res. Lett. **44**, 6933–6939 (2017).
20. R. A. Reynolds, D. Stramski, and G. Neukermans, "Optical backscattering by particles in Arctic seawater and relationships to particle mass concentration, size distribution, and bulk composition," Limnol. Oceanogr. **61**, 1869–1890 (2016).
21. W. M. Balch, B. C. Bowler, D. T. Drapeau, A. J. Poulton, and P. M. Holligan, "Biominerals and the vertical flux of particulate organic carbon from the surface ocean," Geophys. Res. Lett. **37**, L22605 (2010).
22. I. Cetinić, M. J. Perry, N. T. Briggs, E. Kallin, E. A. D'Asaro, and C. M. Lee, "Particulate organic carbon and inherent optical properties during 2008 North Atlantic bloom experiment," J. Geophys. Res. Oceans **117**, C06028 (2012).
23. N. Haëntjens, E. Boss, and L. D. Talley, "Revisiting ocean color algorithms for chlorophyll a and particulate organic carbon in the southern ocean using biogeochemical floats," J. Geophys. Res. Oceans **122**, 6583–6593 (2017).
24. D. Stramski, R. A. Reynolds, M. Kahru, and B. G. Mitchell, "Estimation of particulate organic carbon in the ocean from satellite remote sensing," Science **285**, 239–242 (1999).
25. D. Stramski, R. A. Reynolds, M. Babin, S. Kaczmarek, M. R. Lewis, R. Röttgers, A. Sciandra, M. Stramska, M. S. Twardowski, B. A. Franz, and H. Claustre, "Relationships between the surface concentration of particulate organic carbon and optical properties in the eastern South Pacific and eastern Atlantic Oceans," Biogeosciences **5**, 171–201 (2008).
26. N. T. Briggs, W. H. Slade, E. Boss, and M. J. Perry, "Method for estimating mean particle size from high-frequency fluctuations in beam attenuation or scattering measurements," Appl. Opt. **52**, 6710–6725 (2013).
27. N. Briggs, G. Dall'Olmo, and H. Claustre, "Major role of particle fragmentation in regulating biological sequestration of CO_2 by the oceans," Science **367**, 791–793 (2020).
28. T. S. Kostadinov, D. A. Siegel, and S. Maritorena, "Retrieval of the particle size distribution from satellite ocean color observations," J. Geophys. Res. Oceans **114**, C09015 (2009).
29. W. H. Slade and E. Boss, "Spectral attenuation and backscattering as indicators of average particle size," Appl. Opt. **54**, 7264–7277 (2015).
30. Y. C. Agrawal and H. C. Pottsmith, "Instruments for particle size and settling velocity observations in sediment transport," Mar. Geol. **168**, 89–114 (2000).
31. X. Zhang, M. Twardowski, and M. Lewis, "Retrieving composition and sizes of oceanic particle subpopulations from the volume scattering function," Appl. Opt. **50**, 1240–1259 (2011).
32. M. S. Twardowski, E. Boss, J. B. Macdonald, W. S. Pegau, A. H. Barnard, and J. R. V. Zaneveld, "A model for estimating bulk refractive index from the optical backscattering ratio and the implications for understanding particle composition in case I and case II waters," J. Geophys. Res. Oceans **106**, 14129–14142 (2001).
33. O. Ulloa, S. Sathyendranath, and T. Platt, "Effect of the particle-size distribution on the backscattering ratio in seawater," Appl. Opt. **33**, 7070–7077 (1994).
34. E. Boss, W. S. Pegau, M. Lee, M. Twardowski, E. Shybanov, G. Korotaev, and F. Baratange, "Particulate backscattering ratio at LEO 15 and its use to study particle composition and distribution," J. Geophys. Res. Oceans **109**, C01014 (2004).
35. D. Koestner, D. Stramski, and R. A. Reynolds, "Measurements of the volume scattering function and the degree of linear polarization of light scattered by contrasting natural assemblages of marine particles," Appl. Sci. **8**, 2690 (2018).
36. M. Soja-Woźniak, M. Baird, T. Schroeder, Y. Qin, L. Clementson, B. Baker, D. Boadle, V. Brando, and A. D. L. Steven, "Particulate backscattering ratio as an indicator of changing particle composition in coastal waters: observations from Great Barrier Reef waters," J. Geophys. Res. Oceans **124**, 5485–5502 (2019).
37. A. L. Whitmire, E. Boss, T. J. Cowles, and W. S. Pegau, "Spectral variability of the particulate backscattering ratio," Opt. Express **15**, 7019–7031 (2007).
38. M. Chami, E. B. Shybanov, T. Y. Churilova, G. A. Khomenko, M. E. G. Lee, O. V. Martynov, G. A. Berseneva, and G. K. Korotaev, "Optical properties of the particles in the Crimea coastal waters (Black Sea)," J. Geophys. Res. Oceans **110**, C11020 (2005).
39. M. Babin, A. Morel, V. Fournier-Sicre, F. Fell, and D. Stramski, "Light scattering properties of marine particles in coastal and open ocean waters as related to the particle mass concentration," Limnol. Oceanogr. **48**, 843–859 (2003).
40. D. Stramski, A. Bricaud, and A. Morel, "Modeling the inherent optical properties of the ocean based on the detailed composition of planktonic community," Appl. Opt. **40**, 2929–2945 (2001).
41. D. Stramski, M. Babin, and S. B. Woźniak, "Variations in the optical properties of terrigenous mineral-rich particulate matter suspended in seawater," Limnol. Oceanogr. **52**, 2418–2433 (2007).
42. S. B. Woźniak, D. Stramski, M. Stramska, R. A. Reynolds, V. M. Wright, E. Y. Miksic, M. Cichocka, and A. M. Cieplak, "Optical variability of seawater in relation to particle concentration, composition, and size distribution in the nearshore marine environment at Imperial Beach, California," J. Geophys. Res. Oceans **115**, C08027 (2010).
43. E. S. Fry and K. J. Voss, "Measurement of the Mueller matrix for phytoplankton," Limnol. Oceanogr. **30**, 1322–1326 (1985).
44. O. Muñoz, F. Moreno, D. Guirado, D. D. Dabrowska, H. Volten, and J. W. Hovenier, "The Amsterdam–Granada light scattering database," J. Quant. Spectrosc. Radiat. Transfer **113**, 565–574 (2012).
45. M. S. Quinby-Hunt, A. J. Hunt, K. Lofftus, and D. Shapiro, "Polarized-light scattering studies of marine Chlorella," Limnol. Oceanogr. **34**, 1587–1600 (1989).
46. Ø. Svensen, J. J. Stamnes, M. Kildemo, L. M. S. Aas, S. R. Erga, and Ø. Frette, "Mueller matrix measurements of algae with different shape and size distributions," Appl. Opt. **50**, 5149–5157 (2011).
47. H. Volten, J. F. De Haan, J. W. Hovenier, R. Schreurs, W. Vassen, A. G. Dekker, H. J. Hoogenboom, F. Charlton, and R. Wouts, "Laboratory measurements of angular distributions of light scattered by phytoplankton and silt," Limnol. Oceanogr. **43**, 1180–1197 (1998).
48. P. J. Wyatt and C. Jackson, "Discrimination of phytoplankton via light-scattering properties," Limnol. Oceanogr. **34**, 96–112 (1989).
49. D. Koestner, D. Stramski, and R. A. Reynolds, "Polarized light scattering measurements as a means to characterize particle size and composition of natural assemblages of marine particles," Appl. Opt. **59**, 8314–8334 (2020).
50. D. Stramski, R. A. Reynolds, P. Gernez, R. Röttgers, and O. Wurl, "Inherent optical properties and particle characteristics of the sea-surface microlayer," Prog. Oceanography **176**, 102117 (2019).
51. B. Cochenour, K. Dunn, A. Laux, and L. Mullen, "Experimental measurements of the magnitude and phase response of high-frequency modulated light underwater," Appl. Opt. **56**, 4019–4024 (2017).
52. L. Hu, X. Zhang, and M. J. Perry, "Light scattering by pure seawater at subzero temperatures," Deep–Sea Res. I **162**, 103306 (2020).
53. R. Sahoo, S. K. Sahu, and P. Shanmugam, "Estimation of the channel characteristics of a vertically downward optical wireless communication link in realistic oceanic waters," Opt. Laser Technol. **116**, 144–154 (2019).
54. H. Sandven, A. S. Kristoffersen, Y. Chen, and B. Hamre, "In situ measurements of the volume scattering function with LISST-VSF

and LISST-200X in extreme environments: evaluation of instrument calibration and validity," Opt. Express **28**, 37373–37396 (2020).
55. X. Zhang, L. Hu, Y. Xiong, Y. Huot, and D. Gray, "Experimental estimates of optical backscattering associated with submicron particles in clear oceanic waters," Geophys. Res. Lett. **47**, e2020GL087100 (2020).
56. X. Zhang, L. Hu, D. Gray, and Y. Xiong, "Shape of particle backscattering in the North Pacific Ocean: the χ factor," Appl. Opt. **60**, 1260–1266 (2021).
57. D. Koestner, D. Stramski, and R. A. Reynolds, "Assessing the effects of particle size and composition on light scattering through measurements of size-fractionated seawater samples," Limnol. Oceanogr. **65**, 173–190 (2020).
58. C. F. Bohren, "Multiple scattering of light and some of its observable consequences," Am. J. Phys. **55**, 524–533 (1987).
59. D. Doxaran, E. Leymarie, B. Nechad, A. Dogliotii, K. Kuddick, P. Gernez, and E. Knaeps, "Improved correction methods for field measurements of particulate light backscattering in turbid waters," Opt. Express **24**, 3615–3637 (2016).
60. H. S. Ugulen, H. Sandven, B. Hamre, A. S. Kristoffersen, and C. Saetre, "Analysis of multiple scattering errors in LISST-VSF volume scattering function measurements using Monte Carlo simulations and experimental data," Opt. Express **29**, 12413–12428 (2021).
61. T. R. Parsons, Y. Maita, and C. M. Lalli, *A Manual of Chemical and Biological Methods for Seawater Analysis* (Pergamon, 1984).
62. D. W. van der Linde, "Protocol for the determination of total suspended matter in oceans and coastal zones," Technical note I.98.182 (Joint Research Centre, 1998).
63. M. G. Novak, I. Cetinić, J. E. Chaves, and A. Mannino, "The adsorption of dissolved organic carbon onto glass fiber filters and its effect on the measurement of particulate organic carbon: a laboratory and modeling exercise," Limnol. Oceanogr. Methods **16**, 356–366 (2018).
64. IOCCG Protocol Series, "Inherent optical property measurements and protocols: absorption coefficient," in *IOCCG Ocean Optics and Biogeochemistry Protocols for Satellite Ocean Colour Sensor Validation*, Nova Scotia, Canada (2018), Vol. **1.0**.
65. R. Röttgers and S. Gehnke, "Measurement of light absorption by aquatic particles: improvement of the quantitative filter technique by use of an integrating sphere approach," Appl. Opt. **51**, 1336–1351 (2012).
66. D. Stramski, R. A. Reynolds, S. Kaczmarek, J. Uitz, and G. Zheng, "Correction of pathlength amplification in the filter-pad technique for measurements of particulate absorption coefficient in the visible spectral region," Appl. Opt. **54**, 6763–6782 (2015).
67. M. Kishino, M. Takahashi, N. Okami, and S. Ichimura, "Estimation of the spectral absorption coefficients of phytoplankton in the sea," Bull. Mar. Sci. **37**, 634–642 (1985).
68. J. H. Ahn and S. B. Grant, "Size distribution, sources, and seasonality of suspended particles in Southern California marine bathing waters," Environ. Sci. Technol. **41**, 695–702 (2007).
69. R. A. Reynolds, D. Stramski, V. M. Wright, and S. B. Woźniak, "Measurements and characterization of particle size distributions in coastal waters," J. Geophys. Res. Oceans **115**, C08024 (2010).
70. T. Serra, J. Colomer, X. P. Cristina, X. Vila, J. B. Arellano, and X. Casamitjana, "Evaluation of laser in situ scattering instrument for measuring concentration of phytoplankton, purple sulfur bacteria, and suspended inorganic sediments in lakes," J. Environ. Eng. **127**, 1023–1030 (2001).
71. W. S. Bickel and W. M. Bailey, "Stokes vectors, Mueller matrices, and polarized scattered light," Am. J. Phys. **53**, 468–478 (1985).
72. L. Hu, X. Zhang, Y. Xiong, and M.-X. He, "Calibration of the LISST-VSF to derive the volume scattering functions in clear waters," Opt. Express **27**, A1188–A1206 (2019).
73. X. Zhang, L. Hu, and M.-X. He, "Scattering by pure seawater: effect of salinity," Opt. Express **17**, 5698–5710 (2009).
74. X. Zhang, D. Stramski, R. A. Reynolds, and E. R. Blocker, "Light scattering by pure water and seawater: the depolarization ratio and its variation with salinity," Appl. Opt. **58**, 991–1004 (2019).
75. J. Piskozub, D. Stramski, E. Terrill, and W. K. Melville, "Influence of forward and multiple light scatter on the measurement of beam attenuation in highly scattering marine environments," Appl. Opt. **43**, 4723–4731 (2004).
76. X. Zhang, G. R. Fournier, and D. J. Gray, "Interpretation of scattering by oceanic particles around 120 degrees and its implication in ocean color studies," Opt. Express **25**, A191–A199 (2017).
77. R. R. Sokal and F. J. Rohlf, *Biometry: The Principles and Practice of Statistics in Biological Research*, 3rd ed. (W. H. Freeman and Company, 1995).
78. F. R. Hampel, E. M. Ronchetti, P. J. Rousseeuw, and W. A. Stahel, *Robust Statistics: The Approach Based on Influence* (Wiley, 1986).
79. W. E. Ricker, "Linear regressions in Fishery research," J. Fish. Res. Board Can. **30**, 409–434 (1973).
80. S. Makridakis, "Accuracy measures: theoretical and practical concerns," Int. J. Forecast. **9**, 527–529 (1993).
81. S. K. Morley, T. V. Brito, and D. T. Welling, "Measures of model performance based on the log accuracy ratio," Space Weather **16**, 69–88 (2018).
82. M. I. Mishchenko, J. W. Hovenier, and L. D. Travis, *Light Scattering by Nonspherical Particles: Theory, Measurements, and Applications* (Academic, 2000).
83. A. Quirantes, F. Arroyo, and J. Quirantes-Ros, "Multiple light scattering by spherical particle systems and its dependence on concentration: a T-Matrix study," J. Colloid Interface Sci. **240**, 78–82 (2001).
84. M. Chami, A. Thirouard, and T. Harmel, "POLVSM (polarized volume scattering meter) instrument: an innovative device to measure the directional and polarized scattering properties of hydrosols," Opt. Express **22**, 26403–26428 (2014).
85. J. K. Lotsberg and J. J. Stamnes, "Impact of particulate oceanic composition on the radiance and polarization of underwater and backscattered light," Opt. Express **18**, 10432–10445 (2010).
86. M. I. Mishchenko and L. D. Travis, "Light scattering by polydispersions of randomly oriented spheroids with sizes comparable to wavelengths of observation," Appl. Opt. **33**, 7206–7225 (1994).
87. E. Boss, L. Taylor, S. Gilbert, K. Gundersen, N. Hawley, C. Janzen, T. Johengen, H. Purcell, C. Robertson, D. W. H. Schar, G. J. Smith, and M. N. Tamburri, "Comparison of inherent optical properties as a surrogate for particulate matter concentration in coastal waters," Limnol. Oceanogr. Methods **7**, 803–810 (2009).
88. D. McKee, J. Piskozub, and I. Brown, "Scattering error corrections for in situ absorption and attenuation measurements," Opt. Express **16**, 19480–19492 (2008).
89. Y. Huot, A. Morel, M. S. Twardowski, D. Stramski, and R. A. Reynolds, "Particle optical scattering along a chlorophyll gradient in the upper layer of the eastern South Pacific Ocean," Biogeosciences **5**, 495–507 (2008).
90. D. C. J. Gordon, "Some studies on the distribution and composition of particulate organic carbon in the North Atlantic Ocean," Deep-Sea Res. **17**, 233–243 (1970).
91. G. A. Riley, "Particulate organic matter in sea water," Adv. Mar. Biol. **8**, 1–118 (1970).
92. R. A. Feely, L. Sullivan, and W. M. Sackett, "Light-scattering measurements and chemical analysis of suspended matter in the near-bottom nepheloid layer of the Gulf of Mexico," in *Suspended Solids in Water*, R. J. Gibbs, ed. (Plenum, 1974), pp. 281–293.
93. D. Stramski, "Corrigendum to 'Relationships between the surface concentration of particulate organic carbon and optical properties in the eastern South Pacific and eastern Atlantic Oceans,'" Biogeosciences 5, 171–201 (2008)," Biogeosciences **5**, 595 (2008).
94. D. Koestner, D. Stramski, and R. A. Reynolds, "Polarized light scattering measurements as a means to characterize particle size and composition of natural assemblages of marine particles: erratum," Appl. Opt. **60**, 380–382 (2021).
95. K. R. Barnhart, I. Overeem, and R. S. Anderson, "The effect of changing sea ice on the physical vulnerability of Arctic coasts," Cryosphere **8**, 1777–1799 (2014).
96. A. Newton and J. Weichselgartner, "Hotspots of coastal vulnerability: a DPSIR analysis to find societal pathways and responses," Estuarine, Coastal Shelf Sci. **140**, 123–133 (2014).
97. S. Menden-Deuer, W. H. Slade, and H. M. Dierssen, "Promoting instrument development for new research avenues in ocean science: opening the black box of grazing," Front. Mar. Sci. **8**, 695938 (2021).
98. M. Galí, M. Falls, H. Claustre, O. Aumont, and R. Bernardello, "Bridging the gaps between particulate backscattering measurements and modeled particulate organic carbon in the ocean," Biogeosciences Discuss. [preprint], .